Autophagy 9:9, 1367–1385; September 2013; © 2013 Landes Bioscience

PRKCB/protein kinase C, beta and the mitochondrial axis as key regulators of autophagy

Simone Patergnani,[1] Saverio Marchi,[1] Alessandro Rimessi,[1] Massimo Bonora,[1] Carlotta Giorgi,[1] Kamal D. Mehta[2] and Paolo Pinton[1,*]

[1]Department of Morphology, Surgery and Experimental Medicine; Section of General Pathology; Interdisciplinary Center for the Study of Inflammation (ICSI); Laboratory for Technologies of Advanced Therapies (LTTA); University of Ferrara; Ferrara, Italy; [2]Department of Molecular and Cellular Biochemistry; The Dorothy M. Davis Heart and Lung Research Institute; Ohio State University College of Medicine; Columbus, OH USA

Keywords: protein kinase C β (PRKCB), mitochondria, autophagy, calcium, mitochondrial membrane potential, SHC1/p66

Abbreviations: Ψ_m, mitochondrial membrane potential; AV, autophagic vacuoles; BCL2, B-cell CLL/lymphoma 2; BECN1, Beclin 1, autophagy related; ER, endoplasmic reticulum; FCCP, carbonyl cyanide p-trifluoromethoxyphenylhydrazone; GFP, green fluorescent protein; HEK, human embryonic kidney; IP_3, inositol-1,4,5-triphosphate; KD, kinase-dead; LC3, microtubule-associated protein 1 light chain 3; mETC, mitochondrial electron transport chain complex; MEFs, mouse embryonic fibroblasts; MeS, methyl-succinate; MMP, mitochondrial membrane permeabilization; mPTP, mitochondrial permeability transition pore; MTOR, mechanistic target of rapamycin; PARK2, parkinson protein 2, E3 ubiquitin protein ligase (parkin); PINK1, PTEN-induced putative kinase 1; PRKA, protein kinase A; PRKC, protein kinase C; PMA, phorbol-12-myristate-13-acetate; PRKCA, protein kinase C, alpha; PRKCB, protein kinase C, beta; PRKCG, protein kinase C, gamma; PTEN, phosphatase and tensin homolog; ROS, reactive oxygen species; SQSTM1/p62, sequestosome 1; STS, staurosporine; TMRM, tetramethylrhodamine methyl ester; TSC1, tuberous sclerosis 1; TSC2, tuberous sclerosis 2; VDAC1, voltage-dependent anion channel 1

Autophagy is the major intracellular system of degradation, and it plays an essential role in various biological events. Recent observations indicate that autophagy is modulated in response to the energy status of the mitochondrial compartment. However, the exact signaling mechanism that controls autophagy under these conditions remains unclear. In this study, we report that the activation of protein kinase C β (PRKCB), a member of the classical PRKCs, negatively modulates the mitochondrial energy status and inhibits autophagy. Furthermore, cells treated with a pharmacological PRKCB inhibitor, and *prkcb* knockout MEFs showed an increase in autophagy both in vitro and in vivo, as well as an increased mitochondrial membrane potential (Ψ_m), suggesting a strong involvement of mitochondrial energy in the modulation of the autophagy machinery. Finally, we show that factors that increase the Ψ_m oppose the PRKCB-dependent inhibition of autophagy. Altogether, these data underscore the importance of PRKCB in the regulation of autophagy; moreover, the finding that a pharmacological modulation of the Ψ_m modifies autophagy levels may be useful in fighting pathologies (including various types of cancer and neurodegenerative disorders) that are characterized by reduced levels of autophagy.

Introduction

Macroautophagy (herein "autophagy") is a degradation pathway that is primarily regulated by nutrient starvation. A double-membrane vesicle, called autophagosome, encloses a portion of the cytoplasm, long-lived proteins and organelles and then fuses with a lysosome (to form an autolysosome) for the degradation and consequent recycling of its contents.[1] Autophagy is a major phenomenon of cell biology, acts as a prosurvival or prodeath mechanism and takes part in different biological events, such as protein and organelle turnover, development, aging, pathogen infection, neurodegeneration and cancer.[2-4]

Various tumor suppressor proteins (such as BECN1, PTEN, BH3-only proteins, TSC1 and TSC2) induce autophagy, whereas several oncogenes (such as AKT, PI3K and antiapoptotic proteins from the BCL2 family) simultaneously inhibit it.[5-9] Although PRKCB is not considered to be a classical oncogene, this PRKC family isoform is considered to be a tumor promoter because it enhances certain cellular signaling pathways.[10] For example, the activation of PRKCB promotes phosphorylation of the p66-kilodalton isoform of the growth factor adaptor SHC1/p66 and triggers its mitochondrial accumulation and redox response.[11] Recently, it has been demonstrated that different PRKC isoforms negatively or positively modulate the rate of autophagy,[12-16] but the exact mechanism remains ambiguous, and no information on PRKCB involvement in the autophagic process has been reported. PRKCs are a family of serine/threonine kinases that are involved in tumor formation and progression and are divided into three major groups based on their activating factors: (1) the classical

*Correspondence to: Paolo Pinton; Email: pnp@unife.it
Submitted: 07/13/12; Revised: 05/27/13; Accepted: 05/31/13
http://dx.doi.org/10.4161/auto.25239

(or conventional) PRKC isoforms, α, βI, βII and γ; (2) the novel PRKC isoforms, δ, ε, θ, η and μ; and (3) the atypical PRKC isoforms, ζ and λ.[17] The number of PRKC isozymes expressed and their levels vary in different tissues, and the biological significance for this heterogeneity is not known.[18] However, different PRKC isoforms phosphorylate different target proteins on serine or threonine residues, mediating distinct biological responses.[19,20]

PRKCB localization at the mitochondrial level has been known for some time, and this kinase is implicated in the regulation of mitochondrial integrity and oxidative phosphorylation.[21,22] Mitochondria are the primary energy producers of the cell and are recognized as key participants and transducers of several cell death pathways.[23] Moreover, dysfunctions in mitochondrial physiology contribute to the pathophysiology of several disorders.[24-26]

The energy status of the mitochondria is a fundamental regulator both of starvation-related autophagy (the nonselective catabolism of cellular components, such as the cytosol, organelles and protein aggregates, which occurs upon nutrient deprivation)[27] and of targeted or specific autophagy (the removal of superfluous or damaged organelles and protein aggregates, which occurs under nutrient-rich conditions).[28] However, the role of mitochondrial homeostasis during autophagy remains unclear. Here, we investigate the existence of a putative relationship between PRKCB, mitochondria and autophagy. In the present study, we report that the activation of PRKCB attenuates mitochondrial energy, which in turn reduces autophagy, both in vitro and in vivo. Moreover, we show that the administration of compounds that positively modulate the mitochondrial membrane potential (Ψ_m) reverses the mitochondrial alterations induced by PRKCB activation and rescues the normal rate of autophagy induction. Finally, we suggest the involvement of SHC1 in PRKCB-mediated regulation of autophagic machinery.

Results

PRKCB overexpression attenuates autophagy. The initial goal of our work was to evaluate whether the β isoform of PRKC could affect the autophagy machinery. To unveil this possibility, we quantified the levels of autophagy in HEK293 cells transfected with a PRKCB chimera or with a mock plasmid empty vector as a control.

Microtubule-associated protein 1 light chain 3 (MAP1LC3, hereafter in the text LC3) is a mammalian ortholog of yeast Atg8, which is used as a specific marker to monitor autophagy.[29] After translation, proLC3 (which is neither LC3-I nor LC3-II) is processed to LC3-I, which is localized to the cytosol. After a short stimulatory (e.g., starvation) period, LC3-I is further modified to a cleaved and lipidated membrane-bound form, LC3-II, which is localized to phagophores.[30]

This conversion can be detected by immunoblotting with antibodies against LC3 that recognize the two different forms of LC3: LC3-I possesses a molecular mass of approximately 16 kDa, whereas LC3-II (whose level is correlated with its incorporation into autophagosomes) is 14 kDa in size.[31] In all the experiments, the level of autophagy was quantified as the ratio of LC3-II to ACTB (our loading control) and as the ratio of LC3-II/LC3-I, as it has been recommended in different guidelines for the study of autophagy.[31,32]

The overexpression of PRKCB led to a significant downregulation of autophagy compared with HEK293 cells transfected with empty vector under resting conditions, as assessed by a decrease in the endogenous LC3-II levels, which is indicative of defective autophagy. Furthermore, PRKCB overexpression also inhibits the formation of autophagosomes after serum starvation (**Fig. 1A**). The negative regulation of the autophagic machinery promoted by PRKCB has been also confirmed in control and PRKCB-overexpressing HEK293 cells treated with rapamycin (a MTOR inhibitor), which produces a higher autophagy flux response (**Fig. S1**).

In addition to LC3, it is possible to use the protein SQSTM1/p62 as autophagy marker. In this case, SQSTM1 is inversely correlated with autophagic activity because it is selectively incorporated into autophagosomes via an interaction with LC3; thus, it is efficiently degraded by autophagy.[33,34] The overexpression of PRKCB boosts the abundance of the autophagy substrate SQSTM1, suggesting that this kinase effectively acts as an endogenous inhibitor of autophagy (**Fig. 1A**). To confirm our findings, we performed a live microscopy analysis to monitor the formation of autophagosomes in HEK293 cells that were cotransfected with the PRKCB chimera or empty vector and the green fluorescent protein (GFP)-LC3 reporter. As reported above, the amount of LC3-II is closely correlated with incorporation into autophagosomes and is a marker for the number of autophagosomes; thus, another widely used method of monitoring autophagic activity is the detection of the chimeric protein GFP-LC3. Upon the induction of autophagy, labeled

Figure 1 (See opposite page). PRKCB induces a reduction in the level of autophagy. (**A**) Representative immunoblot of HEK293 cells transfected either with empty vector or with a PRKCB-encoding plasmid and treated (STARV.) or left untreated (resting conditions) with serum-free DMEM. (**B**) HEK293 cells were transfected with a GFP-LC3-encoding plasmid and empty vector (CTRL) or with PRKCB (PRKCB) and cultured in complete medium for 36 h (resting conditions). Where indicated, the cells were starved (STARV.) for 1 h. The bars depict the percentages (means ± standard deviation [SD]) of cells showing the accumulation of GFP-LC3 in puncta. (**C**) PRKCB-expressing or mock-expressing (CTRL) cells were cultured in complete medium for 36 h and treated with or without 20 mM NH_4Cl for 1 h or 2 h. The cell lysates were analyzed for the levels of the specific protein (**i**). Representative statistics of HEK293 cells transiently transfected with mCherry-eGFP-LC3. Where indicated, the cells were cultured in serum-free DMEM (STARV.) or treated with the lysosomotropic agent NH_4Cl (+NH_4Cl). The differences in the autophagic flux were evaluated by counting the total LC3 puncta/cell (Total), yellow LC3 puncta / cell (RFP+GFP+) and red LC3 puncta/cell (RFP+GFP-) for each condition (**ii**). (**D**) Where indicated, HEK293 cells were transfected with a GFP-LC3-encoding plasmid and empty vector (CTRL) or with PRKCA (PRKCA) or with PRKCB (PRKCB) and cultured in complete medium for 36 h to assess the autophagy levels. Before the experiments, the cells were treated with (+his.) or without 5 μM hispidin for 24 h. The bars depict the percentages (means ± SD) of cells showing the accumulation of GFP-LC3 in puncta. (**E**) Quantification of LC3 cleavage and lipidation, by immunoblot with an antibody against LC3 in PRKCA-expressing (PRKCA), PRKCB-expressing (PRKCB) or mock-expressing (CTRL) cells and treated with or without 5 μM hispidin for 24 h (+his.). In all experiments, LC3-II accumulation was quantified by LC3-II/LC3-I and LC3-II/ACTB ratio. **p < 0.01; *p < 0.05.

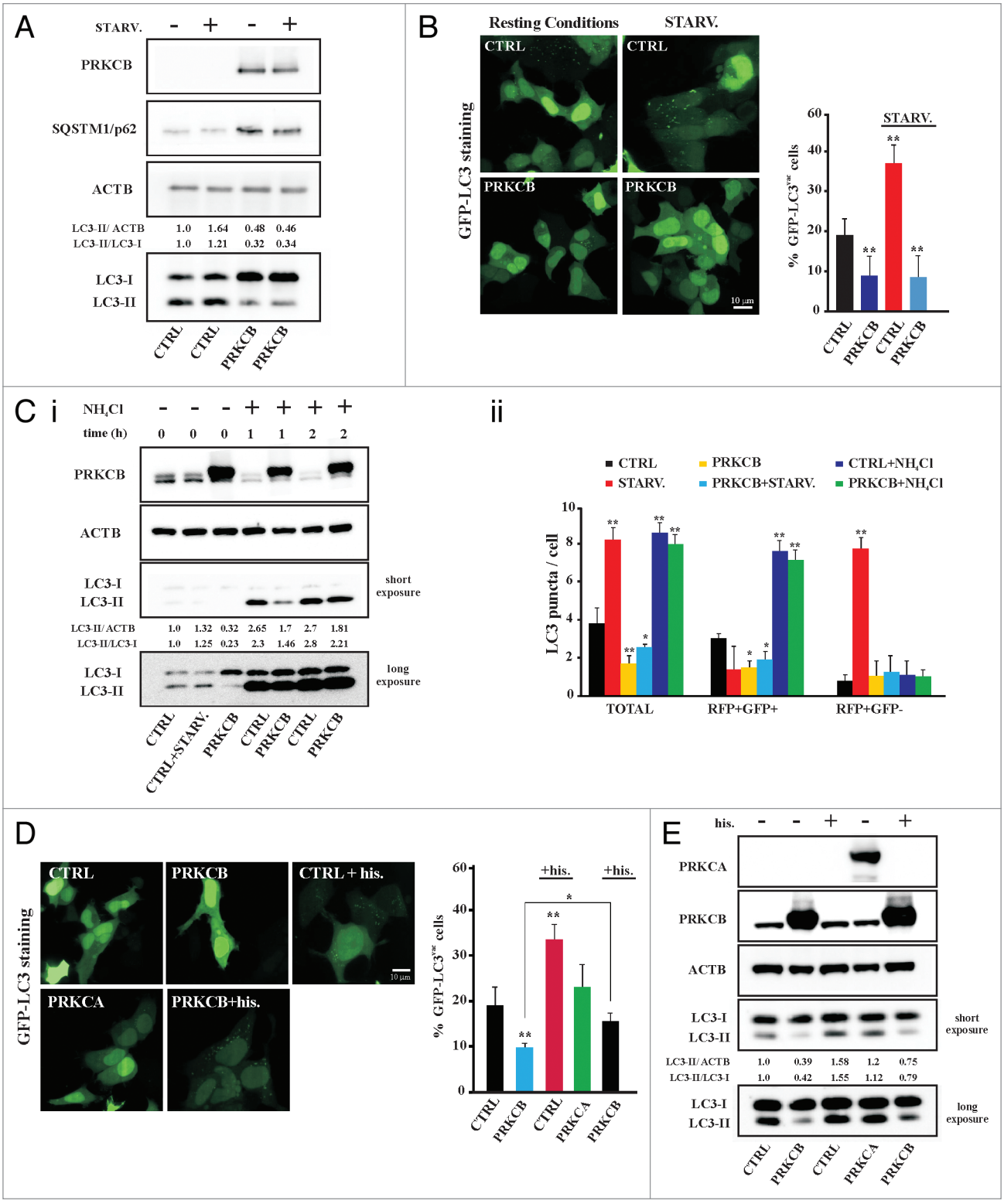

Figure 1. For figure legend, see page 1368.

autophagosomes can be visualized as ring-shaped or punctate structures.[35]

In control cells maintained in resting conditions, LC3 labeling showed a small amount of autophagosomes. After 1 h of serum starvation, many ring-shaped GFP-LC3 structures were observed in control cells, indicating the translocation of LC3-II from the cytosol to autophagic vacuoles (AV). PRKCB-overexpressing cells showed a cytosolic staining pattern for LC3 both under

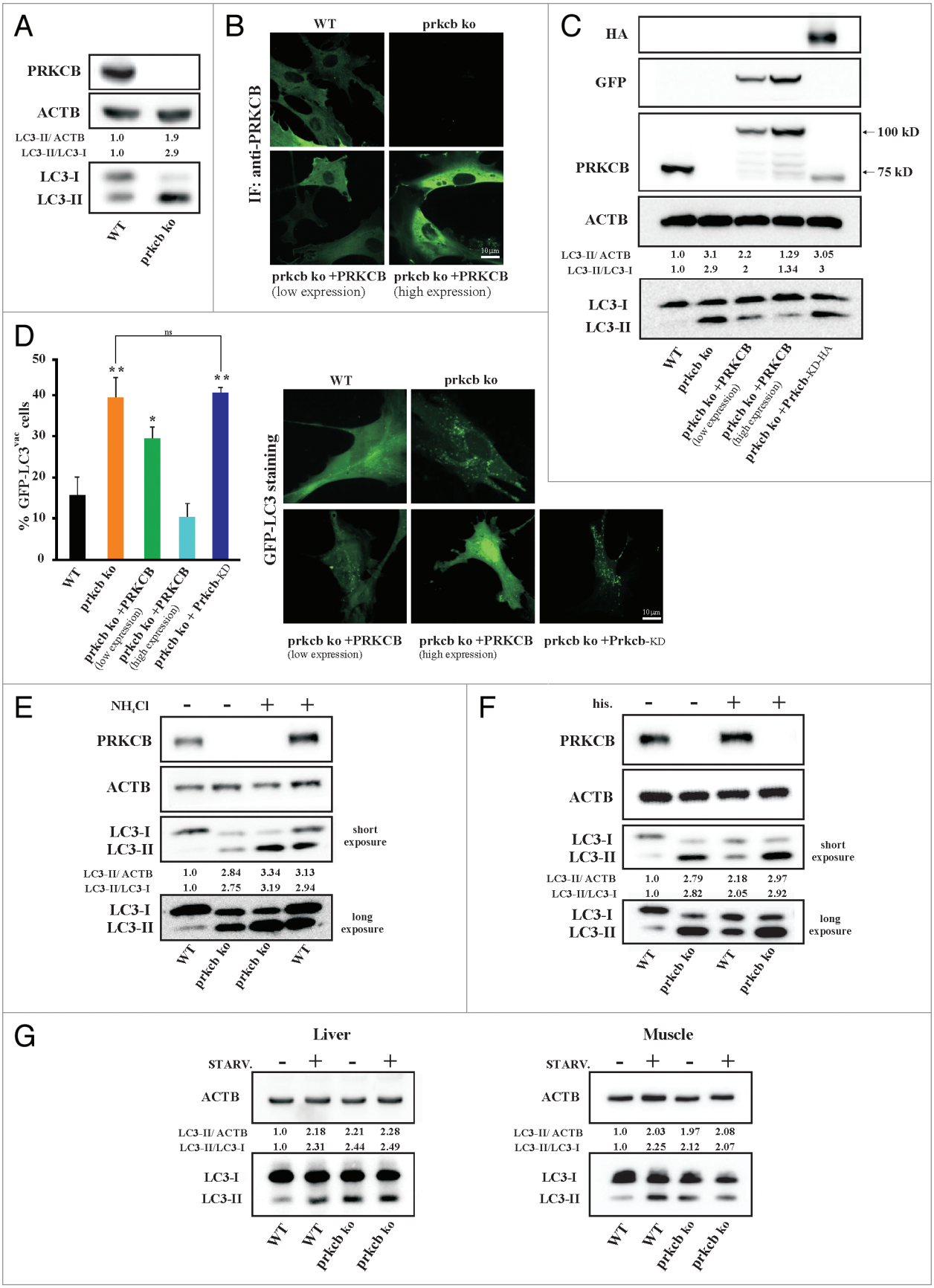

Figure 2. For figure legend, see page 1371.

Figure 2 (See opposite page). Lack of PRKCB promotes the induction of autophagy in vitro and in vivo. (**A**) A representative immunoblot showing the conversion of nonlipidated LC3-I to its cleaved and lipidated variant (LC3-II) in wild-type (WT) and *prkcb* knockout (*prkcb* ko) MEFs. (**B**) The presence/absence of PRKCB in *prkcb* ko MEFs, WT MEFs and *prkcb* ko MEFs expressing PRKCB-GFP was verified by immunostaining using an antibody against PRKCB. (**C**) Western blot of conversion of LC3 in lysates from WT, *prkcb* ko, *prkcb* ko MEFs expressing low (PRKCB low expression) or high (PRKCB high expression) levels of PRKCB-GFP, and *prkcb* ko MEFs expressing *Prkcb*-KD-HA (Prkcb-KD). Immunoblot analysis for GFP identified the presence of PRKCB-GFP. Western blot analysis for HA identified the presence of the kinase-dead, dominant-negative mutant *Prkcb*-KD-HA. ACTB was used as a loading control. (**D**) Cells were transfected with a GFP-LC3-encoding plasmid and empty vector (WT MEF and *prkcb* ko MEF) or with PRKCB (*prkcb* ko MEF expressing PRKCB) or with the kinase-dead dominant-negative mutant *Prkcb*-KD. After 36 h of transfection, the accumulation of GFP-LC3 in puncta was determined. Representative images are shown and quantitative results (means ± SD) are depicted in the graph. (**E**) WT and *prkcb* ko MEFs were cultured in complete medium for 36 h and treated with or without 20 mM NH_4Cl for 1 h. The cell lysates were analyzed for the levels of the specific protein. (**F**) A representative immunoblot of WT and *prkcb* ko MEFs treated (his.+) or left untreated (his.–) with 5 μM hispidin. (**G**) WT and *prkcb* ko mice were fed (STARV.-) or starved (STARV.+) and, after 24 h, the mice were killed and tissues (liver and muscle) were extracted and homogenized. Protein extracts were analyzed for the levels of the specified proteins (n = 3). In all experiments, LC3-II accumulation was quantified by LC3-II/LC3-I and LC3-II/ACTB ratio. **$p < 0.01$; *$p < 0.05$; ns = not significant.

resting conditions and after nutrient withdrawal, confirming that PRKCB plays a critical role as a negative regulator of autophagy (**Fig. 1B**).

The quantification of cellular autophagosomes indicates the level of cellular autophagic activity, but the presence of the autophagosomal marker LC3 can be attributed either to an increased initiation of autophagy or to a block in the degradation of autophagosomes. To distinguish between these possibilities, we performed an autophagic flux assay.[29] In particular, we evaluated the induction of autophagy in the presence of the lysosomal activity inhibitor NH_4Cl. As a result, we found that after a short treatment period (1 h) with NH_4Cl 20 mM in cells expressing PRKCB, the increase in the LC3-II levels was minor comparing treated mock-transfected cells. This suggests that the autophagic response is not compromised in our experimental condition and it is consistent with the ability of PRKCB to attenuate the autophagic process, which in turn led to a minor availability of the cleaved and lipidated form of LC3 (**Fig. 1C, i**). In contrast, after a longer NH_4Cl treatment (2 h) we observed a marked and comparable accumulation of LC3-II either in PRKCB-expressing or control cells, probably due to a saturating level of the lysosomal activity inhibitor (**Fig. 1C, i**).

To confirm this finding, we performed direct fluorescence microscopy to monitor the LC3 turnover in HEK293 cells in the presence of NH_4Cl with the tandem construct mCherry-LC3-eGFP. This assay is based on the concept that the low pH inside the lysosome quenches the signal of GFP, whereas a red fluorescent protein (such as mCherry) is relatively stable in acidic compartments. Thus, most GFP-LC3 puncta do not colocalize with lysosomes. In contrast, mCherry-eGFP-LC3 is detectable in the lysosomal compartment. Thus, it is possible to trace the autophagic flux with the construct mCherry-eGFP-LC3.[35]

LC3 staining under resting conditions showed a small number of autophagosomes and autolysosomes labeled with yellow (RED+GFP+) and red (RED+GFP–), respectively. In starved cells, the number of red puncta (RED+GFP–) was much greater than the number of yellow puncta (RED+GFP+). After treatment with NH_4Cl, the number of yellow puncta (RED+GFP+) was obviously increased without a corresponding increase in red puncta (RED+GFP–), both in control and PRKCB-expressing cells (**Fig. 1C, ii**), suggesting that the accumulation of autophagosomal markers is not due to a block in the degradation of autophagosomes.

To exclude a broad effect of the classic PRKCs and not a specific effect of the β isoform, we performed autophagy measurements in HEK293 cells transfected with the other two conventional PRKC. In agreement with our hypothesis, the overexpression of PRKCA or PRKCG-HA did not modulate autophagy, confirming the specific involvement of PRKCB in the attenuation of autophagy (**Fig. 1D and E**; **Fig. S2**). Finally, to rule out the possibility that we were observing spurious effects of a global perturbation of cellular functions due to the overexpression of PRKCB, we aimed to confirm these observations using the pharmacologic agent hispidin (6-(3,4-dihydroxystyryl)-4-hydroxy-2-pyrone), a specific blocker of the PRKCB isoform.[36] To verify the effective selectivity of hispidin for PRKCB, we performed live fluorescence microscopy analysis to monitor the PRKCB localization. In these experiments, HEK293 cells were transfected with PRKCB-GFP or PRKCA-GFP chimera, treated for 24 h with 5 μM of hispidin and exposed to phorbol-12-myristate-13-acetate (PMA), a strong PRKC activator.

Expression of both PRKCA–GFP and PRKCB–GFP chimeras revealed a bright fluorescence throughout the cytoplasm; meanwhile, after 30 min of treatment with PMA 10 nM, they were localized uniformly in the plasma membrane compartment (PRKCB-GFP: 98 ± 10.3% from control levels, n = 12, $p < 0.01$; PRKCA-GFP: 93 ± 19.5% from control levels, n = 9, $p < 0.01$), as previously reported by us and others.[37-39] Afterwards, we analyzed the behavior of PRKCB and PRKCA upon pretreatment with hispidin. In this case, it is apparent that treatment with PMA induces no change in the distribution of PRKCB (PRKCB-GFP: 5 ± 3.9% from control levels, n = 11) (**Fig.S3, i**), whereas hispidin treatment does not affect the translocation of part of the PRKCA pool to the plasma membrane (PRKCA-GFP: 92 ± 24.6% from control levels, n = 8, $p < 0.01$) (**Fig.S3, ii**). These observations provide evidence that hispidin is a selective inhibitor of the β isoform of PRKC and, as expected, HEK293 cells that were treated for 24 h with 5 μM of hispidin exhibited an increase in autophagy (**Fig. 1D and E**). Moreover, the same treatment with hispidin in PRKCB-overexpressing cells counteracted the negative effect of PRKCB on autophagy, inducing increase both in number of autophagosomes and in LC3-II levels (**Fig. 1D and E**).

Cells lacking PRKCB exhibit enhanced autophagy levels. To confirm the crucial role of PRKCB in the regulation of the autophagy machinery, we assessed autophagy in *prkcb* knockout (ko) MEFs and compared them with wild-type (WT) MEFs. The

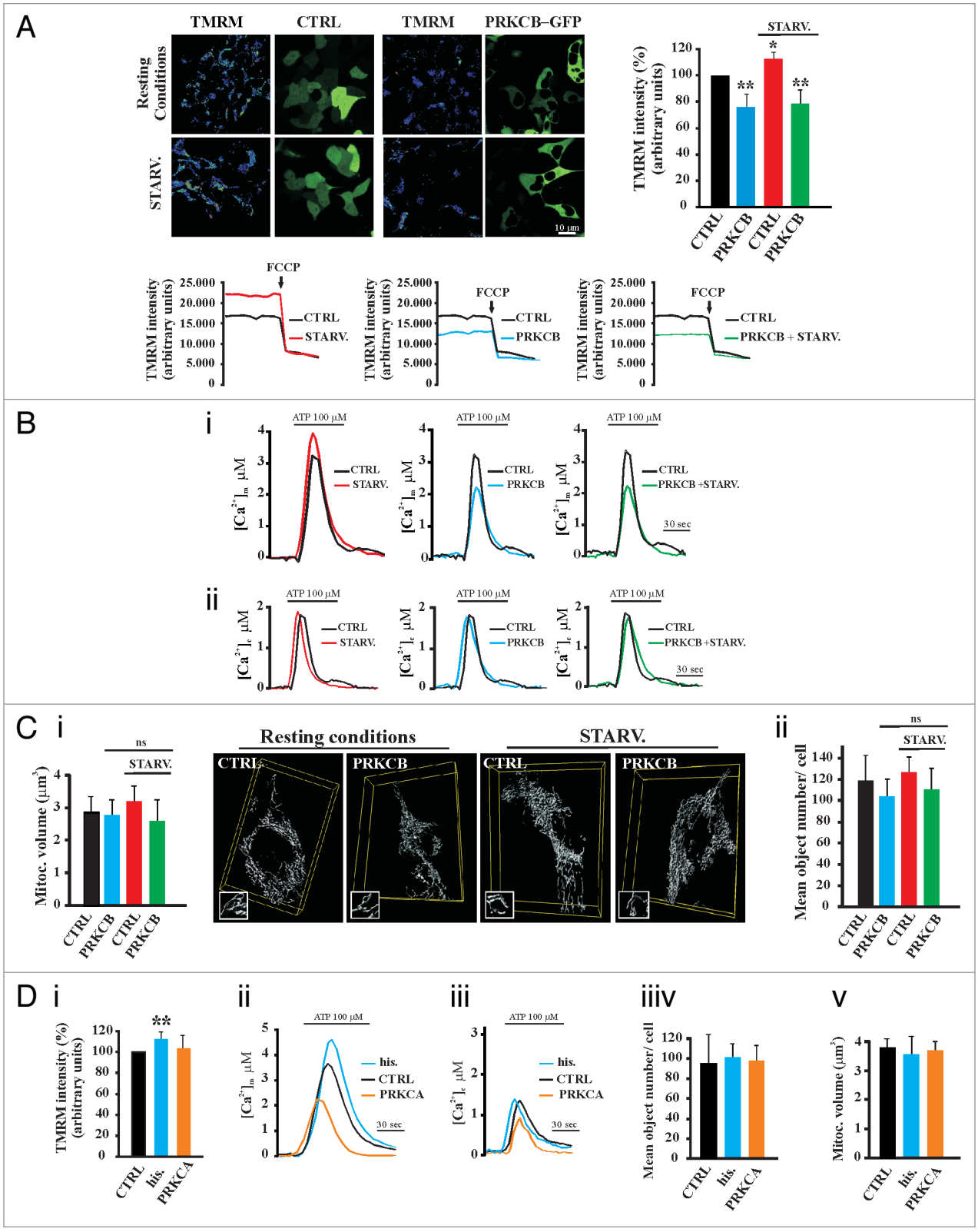

Figure 3. For figure legend, see page 1373

depletion of this kinase induced an accumulation of GFP-LC3 puncta and stimulated the cleavage and lipidation of endogenous LC3, denoting higher autophagy levels in *prkcb* ko than in WT (**Fig. 2A and C–F**). To investigate whether the effects on autophagy were effectively dependent on the absence of PRKCB, we have reintroduced the kinase into *prkcb* ko MEFs, monitoring

also the expression level of the reintroduced gene. First, we assessed by immunocytochemical staining, the expression of isoform β in MEFs when this kinase had been knocked out (**Fig. 2B**). Next, we found that a low expression of the reintroduced *Prkcb* gene restored the autophagy levels relative to those of the wild-type MEFs. Moreover, higher levels of expression of the kinase into *prkcb* ko MEFs resulted in a strong inhibition of autophagy (**Fig. 2C and D**).

As reported above, the changes in autophagosome number can be also caused by perturbation of the normal autophagic activity. To rule out the possibility of a global alteration in the autophagic flux, we evaluated the accumulation of LC3-II after treatment with NH_4Cl. As a result, treatment with 20 mM NH_4Cl for 1 h led to a significant increment of the LC3-II band in *prkcb* ko and wild-type MEFs (**Fig. 2E**). Next, we tested whether the modulation of autophagy observed in HEK293 cells, promoted by hispidin, did not occur in *prkcb* ko MEFs. As expected, a treatment with 5 μM hispidin for 24 h, induced an increase in LC3-II levels in wild-type MEFs, whereas the same experimental conditions achieved on *prkcb* ko MEFs did not modify the autophagic activity compared with *prkcb* ko MEFs (**Fig. 2F**). Finally, to understand whether the kinase activity is a fundamental aspect of PRKCB autophagic role, we used a kinase-dead *Prkcb* HA-tagged construct (*Prkcb*-KD)[40] in *prkcb* ko MEFs and investigated their autophagic levels.

As shown in **Figure 2C** by immunoblot technique and in **Figure 2D** by direct fluorescence microscopy, expression of *Prkcb*-KD did not influence the accumulation of LC3-II band. Similar results were obtained when we performed analyses of autophagy in different tissues (liver and muscle) derived from WT and *prkcb* ko mice under resting conditions and in response to starvation treatment for 24 h (**Fig. 2G**).

Thus, the experiments performed in this more physiological setting show that the knockdown of PRKCB leads to an enhancement of autophagy, confirming that PRKCB plays an essential function in regulation of autophagy, both in vitro (in cultured human and mouse cells) and in vivo (in mice).

PRKCB impairs mitochondrial homeostasis during autophagy. Mitochondria play central roles in cell survival by producing energy through oxidative phosphorylation and in cell death by regulating apoptosis. However, these organelles are also a main source of reactive oxygen species (ROS), which damage cellular components and often induce cell death.[41,42] In healthy cells, complexes I–IV of the respiratory chain build up the proton gradient across the inner mitochondrial membrane that is required for oxidative phosphorylation and that forms the basis of the Ψ_m.[43] The maintenance of this Ψ_m is of vital importance for cellular bioenergetics, and although a transient loss of the Ψ_m can occur in physiological circumstances, a long-lasting or permanent Ψ_m dissipation is often associated with cell death.[44] Based on this understanding, we investigated the role of PRKCB in mitochondrial homeostasis. First, we analyzed the occurrence of Ψ_m changes in PRKCB-GFP-transfected cells compared with control cells (transfected with a GFP reporter), using the mitochondrial potential-sensitive dye tetramethylrhodamine methyl ester (TMRM). As shown in **Figure 3A**, the Ψ_m in the PRKCB-expressing cells (identified by the GFP tag) was drastically smaller than that in the control cells, both when not starved (–21 ± 5.1% from control levels, n = 27, $p < 0.01$) or starved for 1 h (–18 ± 6.8% from control levels, n = 28, $p < 0.01$). By contrast, the starvation treatment performed in the control cells resulted in a significant increase in the Ψ_m (14 ± 4.2% from control levels, n = 36, $p < 0.05$).

The Ψ_m across the inner mitochondrial membrane provides a huge driving force for maintaining a correct amount of mitochondrial calcium (Ca^{2+}).[45] Thus, we performed detailed analyses of the Ca^{2+} homeostasis in HEK293 control cells and cells expressing PRKCB before and after starvation treatment to confirm an effective role of the kinase in mitochondrial physiology. First, using a mitochondrially targeted aequorin,[46] we measured the mitochondrial Ca^{2+} uptake in response to stimulation with ATP, an agonist that triggers IP3-sensitive Ca^{2+} release from the endoplasmic reticulum and the Golgi apparatus, which serve as IP3-sensitive intracellular calcium stores.[47]

Interestingly, starvation treatment in control cells caused a significant increase in the Ca^{2+} uptake by mitochondria (peak amplitude: 3.89 ± 0.6 μM vs. 3.2 ± 0.89 μM [CTRL]; n = 26; $p < 0.05$) (**Fig. 3B, i**); the effect of overexpressed PRKC isoform β on this Ca^{2+} response was different. In fact, similarly to our previous work performed in HeLa cells,[48] in HEK293 cells overexpressing PRKCB, the ATP-dependent mitochondrial Ca^{2+} uptake was significantly reduced, both in untreated (peak amplitude: 2.23 ± 0.3 μM vs. 3.2 ± 0.89 μM [CTRL]; n = 19; $p < 0.01$) and starved cells (peak amplitude: 2.19 ± 0.5 μM vs. 3.2 ± 0.89 μM [CTRL]; n = 20; $p < 0.01$) (**Fig. 3B, i**). We investigated whether the changes in the mitochondrial Ca^{2+} concentration ($[Ca^{2+}]_m$) were paralleled by alterations in the cytosolic Ca^{2+} concentration ($[Ca^{2+}]_c$).

In the experiment shown in **Figure 3B, ii**, we monitored the cytosolic calcium levels in cells expressing either the PRKCB chimera and cytosolic aequorin or the control vector and cytosolic

Figure 3 (See opposite page). PRKCB modulates mitochondrial physiology. (**A**) The mitochondrial transmembrane potential (Ψ_m) of PRKCB-GFP and eGFP (CTRL) cells was detected by the Ψ_m-sensitive probe TMRM. After imaging, the Ψ_m was depolarized by the mitochondrial uncoupler FCCP (black arrows). Where indicated, the cells were starved (STARV.) or not (resting conditions) for 1 h before TMRM loading. Representative images of PRKCB-GFP-expressing (PRKCB-GFP) or eGFP-expressing (CTRL) cells loaded with TMRM are shown; all of the traces are from single representative experiments, and the bars (means ± SD) are quantitative results. (**B**) Mitochondrial (**i**) and cytosolic (**ii**) Ca^{2+} homeostasis measurements with aequorins in mock-transfected (CTRL) and PRKCB-overexpressing (PRKCB) HEK293 cells. Where indicated, the cells were starved (STARV.) or not (resting conditions) for 1 h. (**C**) The mitochondrial number (**i**) and volume (**ii**) as deduced by calculating the object number and size. HEK293 cells were transfected with a red fluorescent protein specifically targeted to the mitochondria (mtDsRed) and empty vector (CTRL) or with PRKCB (PRKCB-overexpressing) and cultured in complete medium for 36 h (resting conditions). Where indicated, the cells were starved for 1 h. Representative images and quantitative results (means ± SD; $p < 0.01$) are depicted. (**D**) Ψ_m (**i**), mitochondrial (**ii**) and cytosolic (**iii**) Ca^{2+} homeostasis measurements with aequorins and mitochondrial number (**iv**) and volume (**v**) in mock-transfected (CTRL) and PRKCA-overexpressing (PRKCA) HEK293 cells. Where indicated, before the experiments, the cells were treated with (his.) or without 5 μM hispidin for 24 h. Representative traces of $[Ca^{2+}]_m$ and $[Ca^{2+}]_c$ peak are shown. **$p < 0.01$; *$p < 0.05$. ns = not significant.

aequorin (control condition) in resting and starvation conditions. No difference was assessed in the $[Ca^{2+}]_c$ between control and PRKCB-overexpressing cells, either not starved (peak amplitude: 1.75 ± 0.28 μM vs. 1.79 ± 0.29 μM [CTRL]; n = 18) or starved for 1 h (peak amplitude: 1.71 ± 0.4 μM vs. 1.79 ± 0.29 μM [CTRL]; n = 18) (**Fig. 3B, ii**). Similar results were obtained when HEK293 cells in control conditions were exposed to serum starvation for 1 h (peak amplitude: 2.03 ± 0.76 μM vs. 1.79 ± 0.89 μM [CTRL]; n = 16) (**Fig. 3B, ii**).

Finally, we wished to rule out the possibility that the alteration of the Ψ_m and of the mitochondrial Ca^{2+} responses were consequences of a major structural perturbation of the organelle that could cause the loss of the ER–mitochondria contact sites, which are essential for the large and prompt Ca^{2+} uptake by mitochondria. The mitochondrial structure was evaluated by confocal microscopy of HEK293 cells that were cotransfected with the PRKCB chimera or empty vector and a mitochondrially targeted red fluorescent protein (mtDsRed). After deconvolution and 3D reconstitution, the images were analyzed, evaluating two main aspects: the overall volume and the size distribution of individual mitochondrial objects. **Figure 3C, i and ii** illustrate that neither the starvation treatment, the overexpression of PRKCB, nor the combination of the overexpression of PRKCB and the starvation treatment affected either the total volume of the mitochondria (122 ± 12 μm^3 [STARV.], 102 ± 17 μm^3 [PRKCB], 110 ± 20 μm^3 [PRKCB+STARV.] vs. 118 ± 24 μm^3 [CTRL]) or the fragmentation of the mitochondrial network (3.18 ± 0.68 μm^3 [STARV.], 2.90 ± 0.72 μm^3 [PRKCB], 2.78 ± 0.91 μm^3 [PRKCB+STARV.] vs. 2.98 ± 0.7 μm^3 [CTRL]). Thus, we concluded that the overexpression of PRKCB (found to inhibit autophagy) negatively modulates mitochondrial activity, as demonstrated by a significant heterogeneity of the Ψ_m and of mitochondrial Ca^{2+} responses compared with control conditions (**Fig. 3A and B**). In contrast, serum starvation (a potent autophagy inducer) enhances mitochondrial bioenergetics, as demonstrated by a significant increase in the Ψ_m, which was reflected in a major mitochondrial Ca^{2+} uptake, not affecting the mitochondrial morphology or the $[Ca^{2+}]_c$ levels (**Fig. 3A and B**).

Next, we aimed to confirm these observations in cells expressing only the endogenous kinase by administering the isoform-specific PRKCB inhibitor hispidin and by upregulating PRKCA to exclude a broad effect of the classic PRKCs. Therefore, we conducted mitochondrial parameter measurements in HEK293 cells that were transfected with PRKCA or treated with hispidin. Treatment with hispidin resulted in an increase in the Ψ_m (+16 ± 4.1% from control levels, n = 16, p < 0.05) (**Fig. 3D, i**), which was reflected in a major change in the $[Ca^{2+}]_m$ (peak amplitude: 4.82 ± 0.74 μM [his.] vs. 3.76 ± 0.34 μM [CTRL] n = 21, p < 0.01) (**Fig. 3D, ii**); in addition, we did not recognize any alteration in $[Ca^{2+}]_c$ or in the mitochondrial size and network (**Fig. 3D, iii and iv**). Next, we assessed a possible change in the Ψ_m levels and the Ca^{2+} response in HEK293 cells expressing PRKC isoform α. The results of the experiment are shown in **Figures 3D, iv and v**. No difference was detected in the loading of the fluorescent dye TMRM (+4 ± 6% from control levels, n = 18) (**Fig. 3D, i**) or in the mitochondrial number (98 ± 18 μm^3 [PRKCA] vs. 95 ± 23 μm^3 [CTRL]) (**Fig. 3D, iv**) and volume (3.76 ± 0.73 μm^3 [PRKCA] vs. 3.86 μm^3 ± 0.81 [CTRL]) (**Fig. 3D, v**) between the control and PRKCA-overexpressing cells. However, this protein kinase C isoform promoted a significant reduction in the mitochondrial calcium uptake compared with the control (peak amplitude: 2.24 ± 0.44 μM [PRKCA] vs. 3.76 ± 0.34 μM [CTRL] n = 14, p < 0.01) (**Fig. 3D, ii**). Next, we investigated whether the $[Ca^{2+}]_m$ changes were paralleled by alterations in the cytosolic Ca^{2+} signals. In PRKCA-transfected cells, the $[Ca^{2+}]_c$ increases evoked by stimulation with an agonist were significantly less than in control cells (peak amplitude: 0.89 ± 0.28 μM [PRKCA] vs. 1.38 ± 0.32 μM [CTRL] n = 22, p < 0.01) (**Fig. 3D, iii**), suggesting the possibility that ER loading (or its discharge properties) was modulated by the activity of PRKCA.

Lack of PRKCB promotes sustained mitochondrial homeostasis. We executed the same experiments in *prkcb* ko MEFs and compared the results with those obtained in MEFs derived from WT mice and in *prkcb* ko MEFs into which *Prkcb* was reintroduced. As reported in **Figure 4A**, we found that *prkcb* ko MEFs (which possess elevated autophagy levels, as reported in **Fig. 2A and C**) exhibited higher Ψ_m levels compared with WT MEFs (+19.5 ± 5.8% from WT levels, n = 21). As expected, a loss of *Prkcb* was reflected in an increase in the mitochondrial Ca^{2+} uptake (peak amplitude: 67.3 ± 3.2 μM [*prkcb* ko] vs. 49.4 ± 4.7 μM [WT] n = 26, p < 0.01) (**Fig. 4B, i**) that affected neither the total volume of the mitochondria nor the structure of the mitochondrial network (**Fig. 4C, i and ii**). Moreover, there were no differences in the $[Ca^{2+}]_c$ (peak amplitude: 1.6 ± 0.18 μM [*prkcb* ko] vs. 1.49 ± 0.23 μM [WT] n = 18) (**Fig. 4B, ii**). Additionally, as reported in **Figure 4A and B**, a low expression of the reintroduced PRKCB-GFP chimera in ko cells restored the Ψ_m levels (TMRM intensity: +6.3 ± 3.8% from WT levels, n = 12) and $[Ca^{2+}]_m$ (peak amplitude: 54.5 ± 4.1 μM vs. 49.4 ± 4.7 μM [WT] n = 13) to values comparable to those in WT MEFs; accordingly, higher level of expression of the kinase into *prkcb* ko MEFs resulted in a significant attenuation of mitochondrial parameters, such as Ψ_m (TMRM intensity: –16.2 ± 2.9% from WT levels, n = 8, p < 0.05) and $[Ca^{2+}]_m$ (peak amplitude of

Figure 4 (See opposite page). Mitochondrial homeostasis in MEFs *prkcb* ko, MEFs WT and MEFs *prkcb* ko expressing a PRKCB chimera. (**A**) Cultured wild-type (WT), *prkcb* knockout (*prkcb* ko) and *prkcb* ko MEFs expressing low (PRKCB low expression) or high (PRKCB high expression) levels of PRKCB-GFP were loaded with TMRM and imaged by confocal microscopy to detect Ψ_m. Representative images and quantitative results (means ± SD) are shown. (**B**) Mitochondrial (**i**) and cytosolic (**ii**) Ca^{2+} measurements. Where indicated, cells infected with adenovirus expressing mitochondrial (mtAEQ) or cytosolic (cytAEQ) targeted aequorin respectively, were stimulated with 100 μM ATP. (**C**) Analysis of mitochondrial structure in cells WT, *prkcb* ko and *prkcb* ko MEFs expressing low (PRKCB low expression) or high (PRKCB high expression) levels of PRKCB-GFP transfected with a red fluorescent protein targeted to the mitochondria (mtDsRed). Images acquired by confocal microscopy were deconvolved, 3D reconstructed and quantitatively analyzed (see Materials and Methods). Representative 3D reconstructed images of mitochondrial morphology are shown. Data represent mean ± SD of mitochondrial number (**i**) and volume (**ii**). **p < 0.01. ns = not significant.

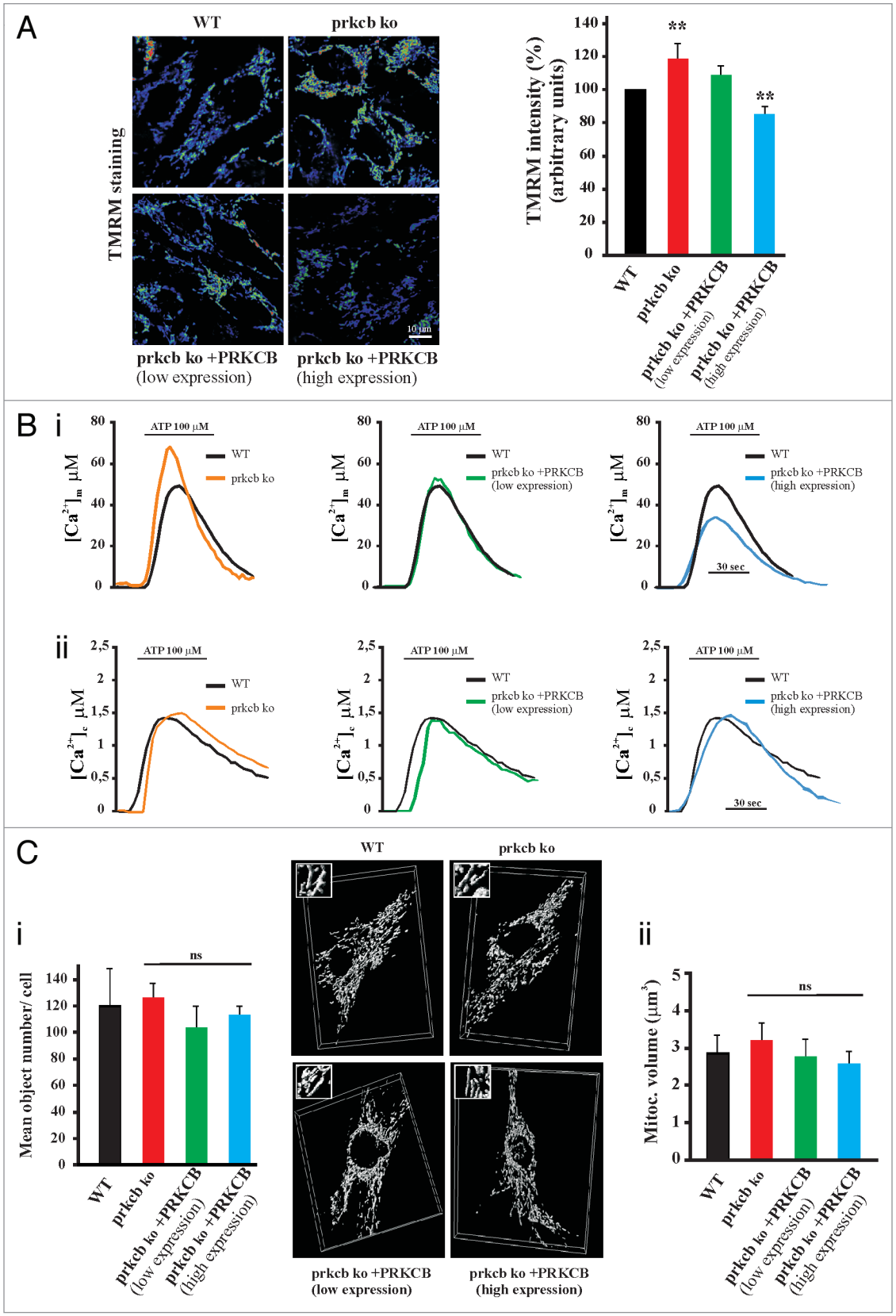

Figure 4. For figure legend, see page 1374.

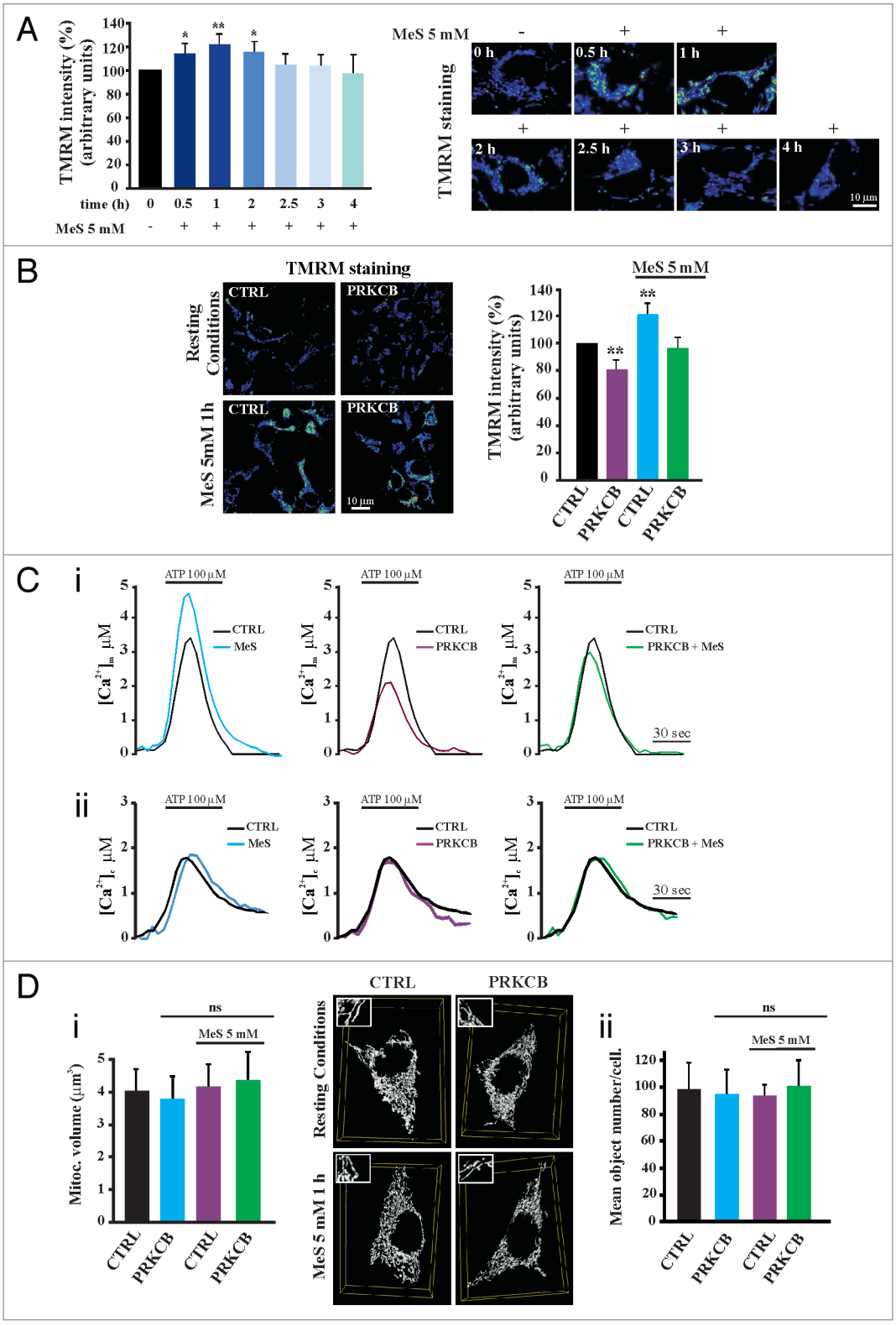

Figure 5. For figure legend, see page 1377

$[Ca^{2+}]_m$ uptake: 36.4 ± 5.1 μM vs. 49.4 ± 4.7 μM [WT] n = 11, $p < 0.05$), without affecting the mitochondrial network (**Fig. 4A–C**).

Overall, these experiments indicate that PRKCB overexpression (a state in which autophagy is attenuated) affects the mitochondrial physiology, inducing a reduction in the Ψ_m and in Ca^{2+} levels. In contrast, the lack of this PRKC or the presence of a condition that activates autophagy (such as serum starvation) positively modulates mitochondrial bioenergetics.

Positive modulation of the Ψ_m contrasts the mitochondrial impairment mediated by PRKCB. As reported above, we have demonstrated that PRKCB selectively attenuates autophagy and impairs mitochondrial physiology without modifying mitochondrial morphology. Next, we asked whether a modulation in mitochondrial homeostasis could reverse the inhibitory effect induced by PRKCB against mitochondrial homeostasis and the autophagy machinery.

An important substrate for mitochondrial function is succinic acid (succinate). Succinate is a substrate for succinate dehydrogenase, which is also known as complex II of the mETC. In contrast to the other enzymes of the Krebs cycle, which are located in the mitochondrial matrix, succinate is bound to the inner mitochondrial membrane.[49] Based on this information, we attempted to modulate mitochondrial physiology with an analogous succinic acid compound, the membrane-permeable methyl-succinate (MeS).[50] First, we tested the efficacy of MeS to modulate mitochondrial bioenergetics, measuring the Ψ_m in mock-transfected and PRKCB-transfected cells in the presence or absence of 5 mM MeS for different time periods (0.5, 1, 2, 2.5, 3 and 4 h) (**Fig. 5A**). As expected, MeS treatment resulted in the hyperpolarization of mitochondria with a peak at approximately 1 h. As illustrated in **Figure 5A**, this effect was maintained until the second hour and subsequently decreased to levels comparable to those of the control. Next, to determine whether MeS could recover the impaired mitochondrial homeostasis induced by the overexpression of PRKCB, we analyzed changes in the Ψ_m in mock-transfected and PRKCB-expressing cells.

The results of the experiment are shown in **Figure 5B**. As reported above, control cells treated with 5 mM of the mETC substrate MeS for 1 h showed higher Ψ_m levels compared with the control. More interestingly, MeS was demonstrated to be able to mitigate the effect induced by PRKCB on the Ψ_m. In fact, PRKCB-expressing cells displayed a reduction in the Ψ_m value (–22 ± 3.2% from control levels, n = 19, $p < 0.01$), but after MeS treatment, the Ψ_m was comparable to the levels found in control cells (–3.2 ± 1.9% from control levels, n = 17) (**Fig. 5B**).

Considering that the enhancement of the Ψ_m generally influences $[Ca^{2+}]_m$, we verified whether MeS could also modify this mitochondrial feature. Thus, we coexpressed the PRKCB chimera or empty vector (control) with aequorin probes, and before taking measurements, we incubated the transfected cells with 5 mM MeS for 1 h. In control cells pretreated with MeS, the $[Ca^{2+}]_m$ increase evoked by ATP stimulation was 4.7 ± 0.87 μM, showing a greater mitochondrial response than the control cells (+34% from control levels, n = 24, $p < 0.01$) (**Fig. 5C, i**). In PRKCB-expressing cells, the mitochondrial Ca^{2+} accumulation was markedly reduced (peak amplitude: 2.04 ± 0.76 μM, n = 23) (**Fig. 5C, i**), but after 1 h of MeS treatment, the mitochondrial calcium uptake was significantly higher (+33.3%, n = 20) (**Fig. 5C, i**) than that observed in PRKCB-expressing cells that were not treated with MeS.

Next, to exclude the possibility of interference with the aequorin signal by MeS, we performed single-cell mitochondrial Ca^{2+} measurements using a version of the GFP-based Ca^{2+} probe Cameleon that is selectively targeted to the mitochondrial matrix (mtCameleon) using live fast microscopy. As expected, treatment with 5 mM MeS affected the mitochondrial Ca^{2+} uptake in both mock-transfected and PRKCB-transfected cells (**Fig. S4**). Moreover, this marked increase induced by MeS was specific to mitochondria, as $[Ca^{2+}]_c$ levels were largely unaffected. In fact, as reported in **Figure 5C, ii**, a pretreatment with 5 mM MeS for 1 h in cells coexpressing the aequorin cytosolic Ca^{2+} probes and the PRKCB chimera (for PRKCB overexpression) or empty vector (control) did not affect the intracellular calcium concentrations (peak amplitude: 1.79 ± 0.34 μM [CTRL], 1.82 ± 0.29 μM [MeS], 1.74 ± 0.52 μM [PRKCB], 1.8 ± 0.44 μM [PRKCB+MeS]; n = 16).

Next, to rule out a possible effect of MeS on mitochondrial morphology, we imaged mtDsRed in the presence of MeS. Either the mitochondrial structure and volume were not significantly altered by treatment with 5mM MeS for 1 h (mitochondria structure: 4.1 ± 0.71 μm^3 [CTRL], 3.81 ± 0.76 μm^3 [MeS], 4.18 ± 0.53 μm^3 [PRKCB], 4.21 ± 0.98 μm^3 [PRKCB+MeS]; n = 24; mitochondria volume: 99 ± 18.3 μm^3 [CTRL], 95 ± 15.8 μm^3 [MeS], 94 ± 7.23 μm^3 [PRKCB], 110 ± 20.2 μm^3 [PRKCB+MeS]; n = 28) (**Fig. 5D, i and ii**).

A sustained Ψ_m positively modulates autophagy and attenuates the inhibitory effects of PRKCB on autophagy. Finally, we sought to determine whether the effect of MeS on mitochondrial physiology could positively modulate autophagy and recover the ability of PRKCB to lower autophagy levels. To examine this possibility, we analyzed autophagy levels and dynamics in HEK293 cells that were exposed to 5 mM of the

Figure 5 (See opposite page). Modulation of Ψ_m recovers the negative effects promoted by PRKCB on mitochondrial metabolism. (**A**) Measurements of Ψ_m in HEK293 with (0.5, 1, 2, 2.5, 3 and 4 h) or without (0 h) MeS 5mM treatment. Quantitative results (means ± SD) and representative images of the TMRM fluorescence after addition of MeS at different times points are shown. (**B**) Quantitative analysis of TMRM fluorescence changes in mock-transfected (CTRL) and PRKCB-overexpressing (PRKCB) HEK293 cells. Representative images and quantitative results (means ± SD) are shown. (**C**) Mitochondrial (**i**) and cytosolic (**ii**) Ca^{2+} homeostasis measurements with aequorins, in mock-transfected (CTRL) and PRKCB-overexpressing (PRKCB) HEK293 cells. Where indicated, cells were incubated with MeS 5 mM for 1 h. Representative traces of $[Ca^{2+}]_m$ and $[Ca^{2+}]_c$ peak are shown. (**D**) Mitochondrial volume (**i**) and number (**ii**) in mock-transfected (CTRL) and PRKCB-overexpressing (PRKCB) HEK293 cells. Where indicated, before experiments, cells were treated with MeS 5 mM for 1 h. Representative 3D reconstructed images of mitochondrial morphology are shown. Data represent mean ± SD of mitochondrial volume (**i**) and number (**ii**). **$p < 0.01$. *$p < 0.05$. ns = not significant.

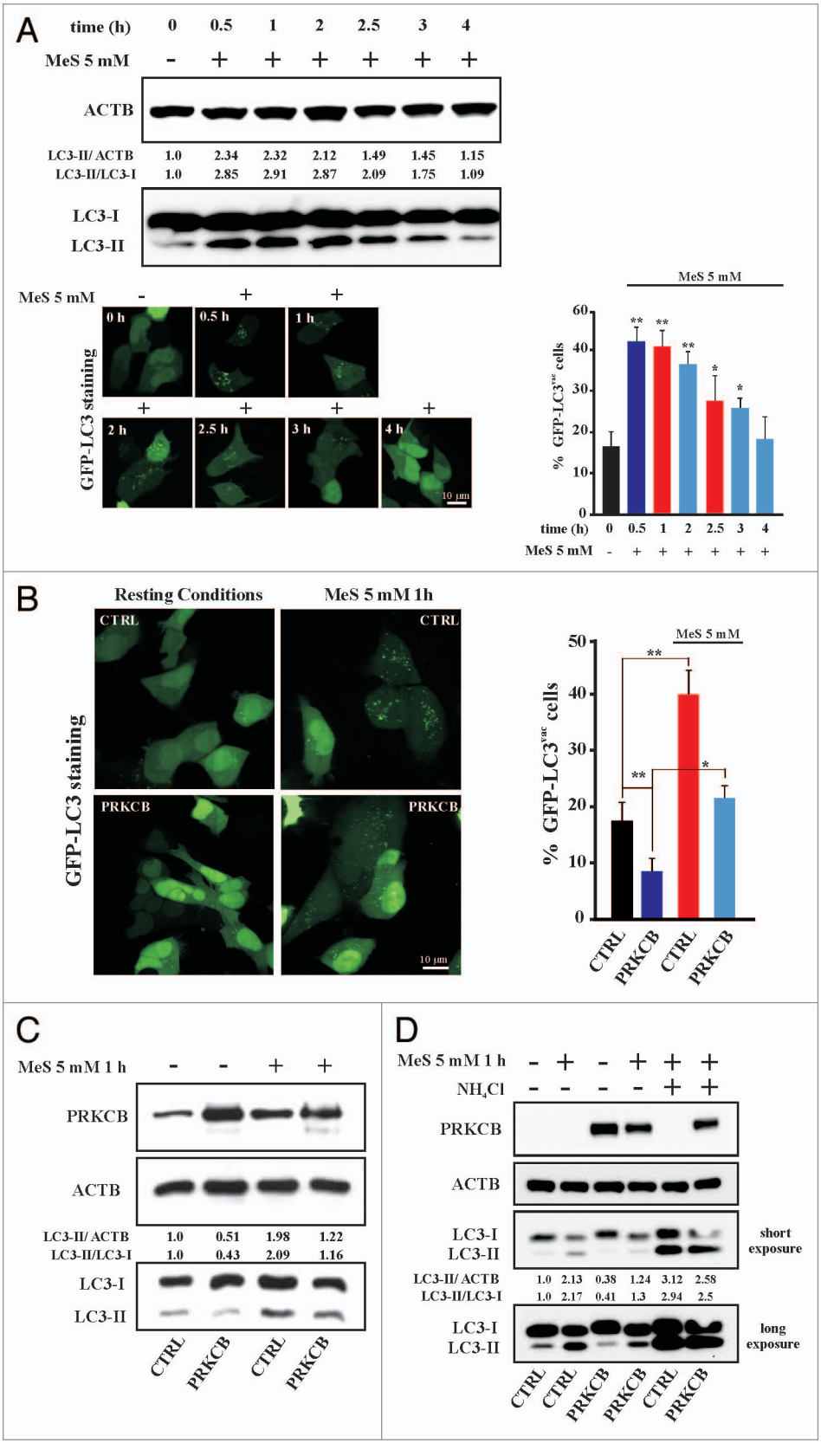

Figure 6. Positive modulation of Ψ_m contrasts the negative effects induced by PRKCB on autophagy. (**A**) Representative LC3-II protein gel blot and GFP-LC3 puncta formation of HEK293 treated with (0.5, 1, 2, 2.5, 3 and 4 h) or without (0 h) MeS 5mM treatment. Quantitative results (means ± SD) and representative images of the GFP-LC3 fluorescence of five independent experiments after addition of MeS at different times points are shown. (**B**) HEK293 cell were transfected with a GFP-LC3-encoding plasmid and empty vector (CTRL) or with PRKCB (PRKCB) and cultured in complete medium for 36 h (Resting conditions). Where indicated, cells were treated with MeS 5mM for 1 h. Bar depict the percentages (means ± SD) of cells showing the accumulation of GFP-LC3 in puncta. (**C**) Representative immunoblot showing the conversion of nonlipidated LC3-I to its cleaved and lipidated variant (LC3-II) in HEK293 cells transfected with empty vector (CTRL) or with PRKCB (PRKCB) (n = 7). (**D**) PRKCB-expressing or mock-expressing (CTRL) cells were cultured in complete medium for 36 h and treated with MeS 5mM for 1 h. Where indicated, cells were treated with or without 20 mM NH_4Cl for 1 h. The cell lysates were analyzed for the levels of the specific protein (n = 5). In all experiments, LC3-II accumulation was quantified by LC3-II/LC3-I and LC3-II/ACTB ratio. **p < 0.01; *p < 0.05.

succinate dehydrogenase compound MeS for different time periods (0.5, 1, 2, 2.5, 3 and 4). Interestingly, the presence of LC3 cleavage and lipidation was maximal after the first and third hour after MeS treatment (**Fig. 6A**). The conversion of the autophagic marker LC3 that was observed via protein gel immunoblotting was also confirmed by the quantification of GFP-LC3 puncta in cells transfected with the chimeric protein GFP-LC3 (**Fig. 6A**).

Having verified that treatment with MeS establishes a positive modulation of autophagy, we measured the level of autophagy by live microscopy, monitoring the formation of autophagosomes in HEK293 cells that were cotransfected with the PRKCB chimera or the empty vector and the GFP-LC3 reporter and then incubated with 5 mM MeS for 1 h. As result, in control cells, treatment with MeS induced higher levels of autophagy,

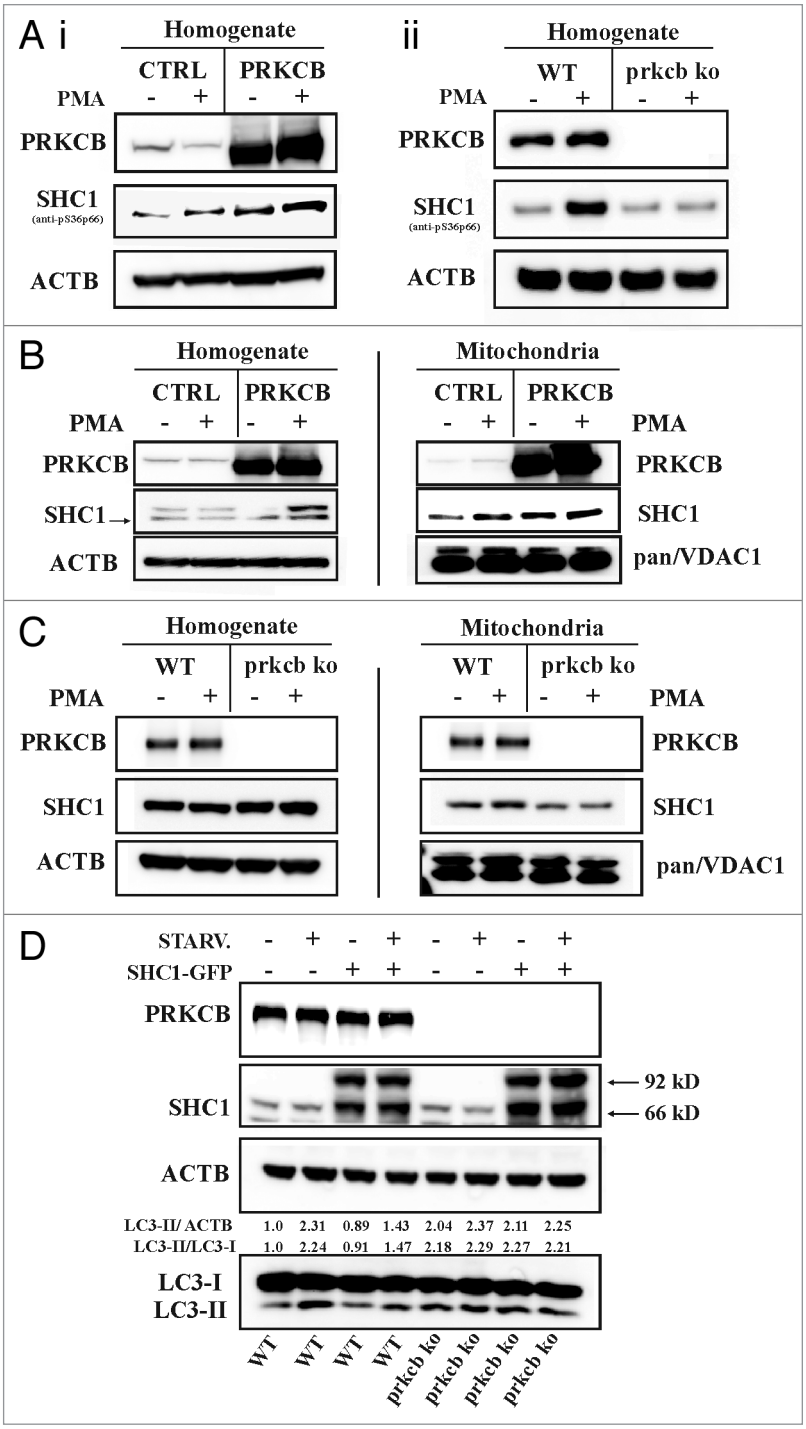

Figure 7. PRKCB-dependent regulation of SHC1 activity as a key aspect in the control of the autophagic process. (**A**) Effects of PRKCB-dependent phosphorylation of SHC1. (**i**) PRKCB-expressing or mock-expressing (CTRL) cells were cultured in complete medium for 36 h and treated with the PRKC activator PMA 10 nM for 30 min. The cell lysates were analyzed for the levels of SHC1 with antibody to SHC1 phosphorylated on Ser36 (anti-pS36p66). (**ii**) Representative western blotting of SHC1 phosphorylated on Ser36 (anti-pS36p66) in MEFs WT and *prkcb* ko treated with PMA 10 nM for 30 min. (**B**) HEK293 cell were transfected with empty vector (CTRL) or with PRKCB (PRKCB), cultured in complete medium for 36 h and subjected to subcellular fraction. Where indicated, cells were treated with PMA 10 nM for 30 min. Immunoblot with antibody to nonphosphorylated SH_2 domain (Src homology 2) of SHC1 identifies the SHC1 protein levels in the mitochondrial fraction. (**C**) Western blot of SHC1 protein levels in the mitochondrial fraction and in the cell homogenate from MEFs WT and *prkcb* ko treated with PMA 10 nM for 30 min. To control for the equal loading of lanes, an anti-ACTB antibody was used (for homogenate) and an anti-pan/VDAC1 (anti-VDAC1) antibody (for mitochondria). (**D**) Effects of SHC1 overexpression on autophagy. Western blot of conversion of LC3 in lysates from MEFs WT, MEFs WT expressing SHC1-GFP, MEFs *prkcb* ko and MEFs *prkcb* ko MEFs expressing SHC1-GFP. Where indicated, the cells were starved (STARV.) with serum-free DMEM (EBSS) for 1 h. Immunoblot analysis for SHC1 identified the presence of SHC1-GFP. In all experiments, LC3-II accumulation was quantified by LC3-II/LC3-I and LC3-II/ACTB ratio. $^{**}p < 0.01$; $^{*}p < 0.05$.

as evidenced by a punctate pattern of GFP-LC3 (40.9 ± 7.1 cells with GFP-LC3^{vac} vs. 16.2 ± 5.2 cells with GFP-LC3^{vac} [CTRL]; n = 32) (**Fig. 6B**). Similar results were observed in PRKCB-expressing cells, where, as expected, GFP-LC3 staining was diffuse within the cytoplasm, with occasional puncta representing a low level of autophagy. Upon MeS treatment, we observed a marked increase in LC3-puncta, suggesting a clear role for MeS both in the modulation of autophagy and, partially, in recovering the ability of PRKCB to reduce autophagy (**Fig. 6B**).

Then, it was fundamental to verify that the MeS treatment did not alter the autophagic process. To reach this goal, we inferred LC3-II-PE turnover by western blot (**Fig. 6D**) in the presence and absence of the lysosomal inhibitor NH_4Cl. Comparing the LC3-II protein abundance during conditions with or without NH_4Cl treatment, we observed that the normal autophagic flux was maintained after MeS treatment. Furthermore, as reported in **Figure 6C**, western blots showing autophagy markers (the LC3-I/-II conversion) confirmed again that these changes were occurring in the whole population of cells. To confirm that the Ψ_m is a fundamental feature of the regulation of autophagy, we treated HEK293 cells with 200 nM staurosporine (STS) for different time periods (0.5, 1, 1.5, 2 and 3 h). STS is reported to positively modulate the Ψ_m, resulting in the hyperpolarization of mitochondria with a peak at approximately 1 h and a subsequent decrease to nearly normal values.[51,52] As expected, under our conditions, we observed a significant increase in the Ψ_m 30 min after STS treatment (**Fig. S5, i**). This effect persisted until 1.5 h and was reflected by an increase in the autophagy, as assessed by LC3-II protein gel immunoblotting (**Fig. S5, ii**). Together, these results suggest that the upregulation of PRKCB leads to a negative modulation of autophagy, whereas the absence of PRKCB promotes an increase in autophagy. Moreover, treatment with MeS, which is capable of positively modulating mitochondrial homeostasis and

particularly the mitochondrial membrane potential, leads to the induction of autophagy and contrasts the negative regulation of autophagy promoted by PRKCB.

Activation and modulation of the 66-kDa isoform of SHC is a key event in PRKCB-mediated autophagy regulation. PRKCB is required for the phosphorylation/activation of SHC1 in Ser36 and for its translocation into the mitochondrial compartment, where it is reported to be a determinant for life span and apoptosis through the perturbation of mitochondrial functions.[11,53] Starting from these observations, we examined whether SHC1 might play a pivotal role in the modulation of autophagy by PRKCB.

At first, we investigated the PRKCB-dependent phosphorylation of SHC1. The levels of phosphorylated SHC1 was detected in HEK293 cells, transfected with PRKCB chimera or with mock plasmid, and treated with the PRKC activator PMA 10 nM for 30 min. Both PRKCB overexpression and PMA treatment led to a significant increase in the levels of phosphorylated SHC1 in Ser36, compared with HEK293 cells transfected with empty vector under resting conditions (**Fig. 7A, i**). Then, to confirm the effective role of PRKCB in the regulation of SHC1 activity, we performed the same experiments in MEFs *prkcb* ko and compared them with MEFs WT. As reported in **Figure 7A, ii**, MEFs WT treated with PMA (10 nM, 30 min) showed a strong increment of phosphorylated SHC1, whereas no significant increase in the levels of the phosphorylated protein has been detected in MEFs *prkcb* ko.

Because SHC1 phosphorylation takes place in the cytoplasm and it is a prior event to its translocation to mitochondria in the unphosphorylated form,[37] we tested the hypothesis that PRKCB activation can modulate the mitochondrial entry of SHC1 protein. For this aim, we evaluated the mitochondrial pool of SHC1 in HEK293 cells that were transfected with the PRKCB chimera or the empty vector, and treated with PMA (10 nM, 30 min). Contemporarily, subcellular fractionations have been performed in MEFs prkcb ko and WT treated or not with the PRKC activator. As a result, the experiments showed that the localization of SHC1 appears to be highly dependent on PRKC activity. In fact, the overexpression of PRKCB chimera and the pharmacological treatment suited for PRKC activation enhanced the transfer of SHC1 to the organelle, whereas cells lacking PRKCB have no detectable effects on the recruitment of SHC1 to mitochondria (**Fig. 7B and C**). Notably, the simple overexpression of PRKCB enhanced both phosphorylation and mitochondrial abundance of SHC1 protein. Next, to investigate whether regulation of SHC1 activity may be a mechanism for autophagy inhibition by PRKCB, we analyzed LC3-II lipidation in *prkcb* ko and WT MEFs, transfected with a SHC1-GFP chimera, in resting condition and after serum starvation. As shown in **Figure 7D**, expression of SHC1-GFP in MEFs WT inhibits autophagy in response to serum starvation, whereas minor effects have been detected in *prkcb* ko cells.

These findings highlight a possible molecular mechanism that links the negative regulation of the autophagic machinery promotes by PRKCB at the PRKCB-dependent mitochondrial translocation of SHC1.

Discussion

In this study, we demonstrated that PRKCB and the mitochondrial axis finely modulate the rate of autophagy. This conclusion is supported by the following observations: (1) overexpression of PRKCB leads to an inhibition of autophagy and induces a decrease in the Ψ_m; (2) a lack of PRKCB stimulates autophagy and induces an increased Ψ_m; (3) nutrient deprivation induces autophagy and promotes a higher Ψ_m that is associated with a stronger mitochondrial Ca^{2+} response to agonist stimulation; (4) the pharmacological increase in the Ψ_m leads to an increase in the level of autophagy; (5) this increase in the Ψ_m not only promotes autophagy but also contrasts with the downregulation of autophagy that is mediated by PRKCB; and (6) SHC1 plays a key role in PRKCB-dependent modulation of autophagy.

Autophagy in mammalian systems occurs under basal conditions and can be stimulated by stresses that include starvation, various pathologies, or treatment with pharmacological agents, such as rapamycin.[54] The autophagy pathway can be an important therapeutic target for diseases such as neurodegeneration and cancer. It is a catabolic pathway that is characterized by the sequestration of cytoplasmic organelles and proteins in double-membrane vesicles (autophagosomes) that fuse with lysosomes, where proteins and organelles are digested by lysosomal hydrolases and are recycled to sustain cellular metabolism.[55]

PRKCB is a member of the protein kinase C (PRKC) family, which consists of several serine/threonine kinases that are divided into three subfamilies on the basis of their general structure and activation requirements.[56] PRKCs play several roles in cell life and survival, especially in regulating cell survival and apoptosis.[37,57,58] Recently, it has been demonstrated that certain PRKC isoforms are crucial for the modulation of autophagy, both in activating and in blocking the pathway.[12-15,59] However, very little is known about the involvement of all PRKC isoforms in autophagy. In the present study, we found that PRKCB significantly attenuates autophagy by modulating mitochondrial homeostasis.

When it was discovered, autophagy was thought to be a nonselective process that randomly recycled intracellular components to compensate for nutrient deprivation.[60] Later on, it was demonstrated that autophagy includes the selective elimination of different organelles, mitochondria in particular (in a process called mitophagy), to maintain quality control and a correct quantity of the organelle and to avoid an excessive accumulation of ROS.[61] In response to several stressors or damage, mitochondrial membrane permeabilization (MMP) occurs, and mitophagy may be initiated to remove these damaged and permeabilized organelles.[62]

To be engulfed by an autophagosome, a mitochondrion has to reach a major axis of approximately 1 μm, compared with the normal value of 5 μm. Thus, it has been suggested that the fragmentation of dysfunctional mitochondria is a crucial step that precedes mitophagy.[63,64] This phenomenon is modulated by a specific ubiquitin ligase, PARK2/parkin[65] and its interaction with the kinase PINK1 (PTEN-induced putative kinase 1).[66] Especially PINK1 undergoes a voltage dependent cleavage

in polarized mitochondria and, following Ψ_m collapse, an accumulation of PINK1 is observed, with consequent induction of PARK2 stabilization and initiation of mitochondrion engulfment. Such a mechanism underlines an important Ψ_m selective role for mitochondrial processing during mitophagy.

However, it has also been demonstrated that nutrient depletion induces the elongation of mitochondria and the maintenance of mitochondrial ATP production, which in turn acts as an escape from mitophagy.[27,67] This event was demonstrated to be dependent on PRKA (protein kinase A) activity, a well known nutrient-sensing mitochondrial kinase.[68,69] In agreement with these findings, our results indicated that autophagy induction by serum starvation preserves the mitochondrial network (**Fig. 3C**) and generates an increase in the mitochondrial energy level, as demonstrated by higher Ψ_m and consequent major mitochondrial Ca^{2+} uptake (**Fig. 3A and B, i**).

Positive or negative regulation of the Ψ_m is a critical parameter of many human diseases, and several exogenous agents can modulate it.[43] Among these agents, STS induces a significant increase in the Ψ_m within 0.5 h to 1 h of treatment, which then remains elevated for approximately 1 h.[52,70] Having ascertained the effective STS-dependent modulation of the Ψ_m in our experimental conditions (**Fig. S3, i**), we recognized a boost in the induction of autophagy that was directly correlated with the modulation of the Ψ_m promoted by STS (**Fig. S3, ii**). A similar effect has been shown on MCF7 cells, displaying increased mitochondrial membrane potential after autophagy induction by exposure to rapamycin.[71] These observations suggest that autophagy induction promotes mitochondrial network bioenergetic activity. Activation of PRKCB leads to a reduction in mitochondrial bioenergetics, which reflects a strong attenuation of autophagy without affecting mitochondrial morphology (**Fig. 3A–C**). Accordingly, we demonstrated that cells lacking *Prkcb* (*prkcb* ko MEFs) and cells treated with a pharmacological PRKCB inhibitor showed an increase in autophagy (**Fig. 1E**; **Fig. 2A–C**) and a sustained mitochondrial physiology (**Fig. 3D**; **Fig. 4A and B**). Thus, it appears that the status of mitochondrial energy is deeply involved in the modulation of the autophagy machinery. Driven by these premises, we attempted to modulate the Ψ_m levels by treatment with MeS, a membrane-permeant methyl ester of succinate. As expected, MeS treatment generates a hyperpolarization of the Ψ_m, which is reflected in an increase in $[Ca^{2+}]_m$ without affecting the mitochondrial network and the global intracellular Ca^{2+} homeostasis, as revealed by the $[Ca^{2+}]_c$ measurements (**Fig. 5**). Our observations that the fine modulation of the Ψ_m positively or negatively impacts the autophagy rate suggest an additional role for this modulator of the mitochondrial electron transport chain. In fact, we showed that MeS treatment stimulates autophagy, partially restores the defective status of mitochondrial energy and the inhibition of autophagy that is induced by the activation of PRKCB. Considering that MeS treatment was not able to completely overcome PRKCB effect on Ψ_m and autophagy, we suppose that mitochondrial PRKCB-activity is not the only mechanism for autophagy regulation by such kinase, but, at least in this cellular model, a relevant one. Indeed, data obtained with MeS and STS confirmed the positive correlation between autophagy and Ψ_m. This evidence contrasts with other works describing the abolition of Ψ_m as general inducer of autophagy or mitophagy. Our results were obtained analyzing the whole energetic status of the mitochondrial network, without considering eventual single-mitochondrion selective mitophagic events. It could be then speculated that the observed prolonged elevation of Ψ_m might generate localized increased ROS production, mPTP opening and mitophagic events, therefore promoting organelle recycling events already addressed to mitophagy.[72]

Studies are underway to identify upstream regulators and downstream targets of PRKCB activation that occur during autophagy. Previously, we reported that PRKCB regulates mitochondrial physiology favoring phosphorylation and mitochondrial translocation of the adaptor protein SHC1, where it interacts with cytochrome c, a component of the electron transport chain, and increases ROS generation.[37] In the present work, we showed that SHC1 expression attenuates autophagy in response to starvation, an effect which has not been observed in *prkcb* ko MEFs (**Fig. 7D**). Thus, both PRKCB and SHC1 overexpression negatively regulate autophagy, and their activity on the process appears linked. In fact, *prkcb* ko cells display very low activity of SHC1, expressed as SHC1 phosphorylation and its abundance at mitochondrial level (**Fig. 7A and C**). We propose a novel role of PRKCB in the control of the autophagic process, through the attenuation of mitochondrial homeostasis and the regulation of mitochondrial SHC1 activity. It has been reported how LC3 staining in neurons was enhanced by blocking SHC1 activation after preconditioning,[73,74] and how PMA treatment, which induces PRKCB activation and SHC1 entry into mitochondria, strongly inhibits autophagy.[14] By this way, SHC1 ko cells should display higher levels of autophagy and this would correlate the increased life span observed in SHC1 ko mice with the proposed prosurvival role of autophagy.[2]

In conclusion, the identification of PRKCB as negative regulator of autophagy through the reduction of the Ψ_m and the regulation of the SHC1 translocation to mitochondria could shed light on the relationship between autophagy and mitochondrial physiology.

Materials and Methods

Cell culture and transfection. Human embryonic kidney HEK293 cells and mouse embryonic fibroblast (MEF) were maintained in a humidified 5% CO_2, 37°C incubator in Dulbecco's modified Eagle's medium (DMEM) supplemented with 10% fetal bovine serum (FBS; Life Technologies, 10270) 100 U/ml penicillin (EuroClone, 3001D), 100 mg/ml streptomycin (EuroClone, 3000D). HEK293 were transfected with a standard calcium phosphate procedure with the following plasmids: PRKCB, PRKCB-GFP, PRKCA, PRKCA-GFP, PRKCG-HA[40] (Addgene plasmid 21236) and GFP-LC3. MEF were transfected using JetPEI (Polyplus transfection™, 101-10) with the plasmid *Prkcb*-kinase-dead (KD)-HA tagged (Addgene plasmid 16385) or with the plasmid SHC1-GFP, or infected by recombinant adenovirus expressing mitochondrially and cytosolic targeted aequorin,

PRKCB-GFP and GFP-LC3. For aequorin measurements, the cells were seeded before transfection onto 13 mm glass coverslips and allowed to grow to 50% confluence. For immunostaining, mitochondrial morphology analysis, PRKCs localization, autophagy measurements by fluorescence microscopy and single cells $[Ca^{2+}]_m$ measurements, cells were seeded on 24 mm glass coverslips. For immunoblotting analysis, cells were seeded on 6-well plates in the same conditions of growth.

Aequorin measurements. Probes used are chimeric aequorins targeted to the cytosol (cytAEQ) and mitochondria (mtAEQmut). For the experiments with cytAEQ and mtAEQmut, cells were incubated with 5 mM coelenterazine (Fluka, 7372) for 1–2 h in DMEM supplemented with 1% FBS. A coverslip with transfected cells was placed in a perfused thermostated chamber located in close proximity to a low-noise photomultiplier with a built-in amplifier/ discriminator.

All aequorin measurements were performed in KRB supplemented with 1 mM $CaCl_2$. Agonist was added to the same medium as specified in figure legends. The experiments were terminated by lysing cells with 100 mM digitonin in a hypotonic Ca^{2+}-containing solution (10 mM $CaCl_2$ in H_2O), thus discharging the remaining aequorin pool. The output of the discriminator was captured by a Thorn EMI photon-counting board and stored in an IBM-compatible computer for further analyses. The aequorin luminescence data were calibrated offline into $[Ca^{2+}]$ values using a computer algorithm based on the Ca^{2+} response curve of wild-type and mutant aequorins.

Antibodies and reagents. For immunoblot and immunostaining analysis, the following antibodies were used: anti-HA (Covance, MMS-101P), anti-LC3B (Sigma-Aldrich, L7543), anti-ACTB (Sigma-Aldrich, A2668), anti-PRKCB (SantaCruz, sc-210; BD 610128), anti-GFP (Roche, 11 814 460 001), anti-PRKCA (SantaCruz, sc-8393), anti-SQSTM1/ p62 (Sigma-Aldrich, P0067), anti-SHC1 (anti-pS36p66; Calbiochem, 566807), anti-SHC1 (BD, 610878), anti-VDAC1 (pan/VDAC Abcam AB, 15895). Other chemicals used are the following: methyl-succinate (MeS; Sigma-Aldrich, M81101), ammonium chloride (NH_4Cl; Sigma-Aldrich, A4514), rapamycin (RAPA.;Calbiochem CAS, 53123-88-9), phorbol-12-myristate-13-acetate (PMA; Sigma-Aldrich, P8139), Earle's Balanced Salt Solution (EBSS; Sigma-Aldrich, E2888).

Immunoblotting. For immunoblotting, cells were scraped into ice-cold, phosphate-buffered saline and lysed in a modified 10 mM Tris buffer pH 7.4 containing 150 mM NaCl, 1% Triton X-100, 10% glycerol, 10 mM EDTA and protease inhibitor cocktail. After 30 min of incubation on ice, the lysates were cleared via centrifugation centrifuged at 12,000 g at 4°C for 10 min. Protein concentrations were determined by the Bio-Rad procedure. Protein extracts, 25 μg, were separated on 4–12% Bis-Tris acrylamide and 4–20% Tris-Glycine Gel (Life Technologies, NP0323 and EC6026) and electron-transferred to PVDF or nitrocellulose membrane according to standard procedures. Unspecific binding sites were saturated by incubating membranes with TBS-Tween 20 (0.05%) supplemented with 5% nonfat powdered milk for 1 h. Next, the membranes were incubated overnight with primary antibodies and the revelation was assessed by the employment of appropriate HRP-labeled secondary antibodies [Santa Cruz, sc-2004 (goat anti-rabbit) and sc-2005 (goat anti-mouse)] plus a chemiluminescent substrate (Thermo Scientific, 34080). To control the equal loading of lanes, it was used an anti-ACTB antibody.

Immunofluorescence. MEFs WT, MEFs *prkcb* ko and MEFs *prkcb* ko cells infected with an adenoviral vector driving PRKCB-GFP expression were washed with PBS, fixed in 4% formaldehyde for 10 min and washed with PBS. Then, cells were permeabilized for 10 min with 0.1% Triton X-100 in PBS and blocked in PBS containing 2% BSA and 0.05% Triton X-100 for 1 h. Cells were then incubated with primary antibody (anti-PRKCB) for 3 h at room temperature and washed three times with PBS. The appropriate isotype-matched, AlexaFluor-conjugated secondary antibodies [Life Technologies, A11008 (488 goat anti-rabbit) and A11001 (488 goat anti-mouse)] were used. Images were taken with a Nikon Swept Field Confocal equipped with CFI Plan Apo VC60XH objective (numerical aperture, 1.4) (Nikon Instruments) and an Andor DU885 electron multiplying charge-coupled device (EM-CCD) camera (Andor Technology Ltd.).

Isolation of mitochondria. Cells were washed twice with PBS, resuspended, and homogenized in a buffer containing 250 mM sucrose, 1 mM EGTA, 50 mM TRIS-HCl, 1 mM DTT, protease inhibitor cocktail, pH 7.4 with 40 μg of digitonin per ml in a glass homogenizer. Homogenate was centrifuged at 1,500 x g for 5 min twice. The final supernatant was collected and centrifuged at 10,000 g for 10 min; the mitochondrial pellets were resuspended with homogenization buffer (without digitonin) and centrifuged again at 10,000 g for 10 min. Mitochondrial pellets were disrupted in 100 μl lysis buffer at 4°C, incubated 30 min on ice and then centrifuged at 17,000 g for 30 min. Protein concentration in the supernatant was determined by the Bio-Rad protein assay kit. To control the equal loading of lanes, we used an anti-ACTB antibody (for homogenate) and an anti-pan/ VDAC1 (anti-VDAC1) antibody (for mitochondria).

Mouse experiments and tissue processing. Prkcb WT and *prkcb* ko mice[75] were bred and maintained according to both the Federation for Laboratory Animal Science Associations and the Animal Experimental Ethics Committee guidelines. They were housed in a temperature-controlled environment with 12 h light dark cycles and received food and water ad libitum. For studies of effects of starvation, mice were deprived of food for 24 h. These mice had free access to drinking water. After killing, mice tissues were homogenized in a 20 mM Tris buffer, pH 7.4, containing 150 mM NaCl, 1% Triton X-100, 10 mM EDTA and protease inhibitor cocktail. Tissue extracts were then centrifuged at 12,000 g at 4°C for 10 min. Protein extracts, 15 μg, were subjected to SDS-PAGE and immunoblotting. Quantification of intensities of the immunoreactive bands was performed using ImageQuant™ LAS-4000 chemiluminescence imaging system (GE Healthcare).

Measurements of mitochondrial Ψ_m. Mitochondrial Ψ_m was measured by loading cells with 20 nM tetramethyl rhodamine methyl ester (TMRM; Life Technologies, T-668) for 30 min at 37°C. Images were taken on an inverted microscope (Nikon LiveScan Swept Field Confocal Microscope (*SFC*) Eclipse Ti

equipped with NIS-Elements microscope imaging software, Nikon Instruments). TMRM excitation was performed at 560 nm and emission was collected through a 590 to 650 nm band-pass filter. Images were taken every 5 s with a fixed 20 ms exposure time. FCCP (carbonyl cyanide p-trifluoromethoxyphenylhydrazone, 10 μM), an uncoupler of oxidative phosphorylation, was added after 12 acquisitions to completely collapse the electrical gradient established by the respiratory chain.

Fluorescence microscopy and quantitative analysis of GFP-LC3 dots. HEK293 cells were cultured in a 24 mm glass coverslips and transfected at 50% confluence with 6 μg of plasmid DNA (control cells: 4 μg pcDNA3 + 2 μg GFP-LC3; PRKC-overexpressing cells: 4 μg PRKC + 2 μg GFP-LC3). MEFs WT, MEFs *prkcb* ko and MEFs *prkcb* ko expressing PRKCB, were cultured in a 24 mm glass coverslips and transfected at 50% confluence: MEF WT and MEFs *prkcb* ko: 4 μg pcDNA3 + 2 μg GFP-LC3; MEFs *prkcb* ko expressing *Prkcb*: 4 μg *Prkcb* + 2 μg GFP-LC3 (for high expression); 2 μg *Prkcb* + 2 μg GFP-LC3 (for low expression); MEFs prkcb ko expressing Prkcb-KD: 4 μg Prkcb-KD + 2 μg GFP-LC3. After 36 h, images were taken on a *Nikon* LiveScan Swept Field Confocal Microscope (*SFC*) Eclipse Ti equipped with NIS-Elements microscope imaging software (Nikon Instruments). For each condition, the number of GFP-LC3 dots was counted in at least 25 independent visual fields.

Mitochondrial morphology analysis. HEK293 cells were seeded before transfection onto 24 mm glass coverslips, allowed to grow to 50% confluence and then transfected with 6 μg of plasmid DNA (control cells: 4 μg pcDNA3 + 2 μg mtDsRed; PRKC-overexpressing cells: 4 μg PRKC + 2 μg mtDsRed). MEFs WT, MEFs *prkcb* ko and MEFs *prkcb* ko expressing PRKCB-GFP, were cultured in a 24 mm glass coverslips and transfected at 50% confluence: MEF WT and MEFs *prkcb* ko: 4 μg pcDNA3 + 2 μg mtDsRed; MEFs prkcb ko expressing Prkcb: 4 μg Prkcb-GFP + 2 μg mtDsRed (for high expression); 2 μg Prkcb-GFP + 2 μg mtDsRed (for low expression). After 36 h expression cells were treated as described then imaged with a Nikon Swept Field confocal equipped with CFI Plan Apo VC60XH objective (n.a. 1.4) (Nikon Instruments) and an Andor DU885 EM-CCD camera (Andor Technology Ltd.). Coverslips were placed in an incubated chamber with controlled temperature, CO_2 and humidity then 51 planes z-stacks where acquired with a voxel dimension of 133 × 133 × 200 nm (X × Y × Z). The mitochondrial network was then described in number and volume using the 3D object counter available in software Fiji (http://fiji.sc/wiki/index.php/Fiji, last accessed June 20, 2011) while 3D renders were obtained with the 3D Viewer plugin.

FRET-based measurements of mitochondrial Ca^{2+}. Single-cell measurements of mitochondrial Ca^{2+} were performed in HEK293 cells transfected with 4mtD3cpv. After 36 h, cells were imaged on a Zeiss Axiovert 200M microscope with a cooled CCD camera (Photometrics), equipped of a C-apochromat 40×/1.2 W CORR objective and controlled by METAFLUOR 7.0 Software (Universal Imaging). Emission ratio imaging of the *cameleon* was accomplished by using a 436DF20 excitation filter, a 450 nm dichroic mirror, and two emission filters (475/40 for ECFP and 535/25 for citrine) controlled by a Lambda 10-2 filter changer (Sutter Instruments). Fluorescence images were background corrected. Exposure times were typically 100 to 200 ms, and images were collected every 5 to 15 s.

Quantitative analysis of the autophagic-flux. HEK293 cultured on 24 mm glass coverslips were transfected with 6 μg of plasmid DNA (control cells: 4 μg pcDNA3 + 2 μg mCherry-eGFP-LC3; PRKCB-overexpressing cells: 4 μg PRKCB + 2 μg mCherry-eGFP-LC3). After 36 h expression cells were treated as described and then imaged on a *Nikon* LiveScan Swept Field Confocal Microscope (*SFC*) Eclipse *Ti* with a 60× magnification and equipped of NIS-Elements microscope imaging software (Nikon Instruments). Obtained puncta image were merge to compare the RFP signals with GFP signals using ImageJ software. For each condition, the colocalization of these two signals was determined by manual counting of fluorescent puncta in at least 20 independent visual fields.

Microscopic analysis of PRKCs translocation. HEK293 cells cultured on 24 mm glass coverslips were transfected with plasmid encoding PRKCA-GFP and PRKCB-GFP. After 36 h expression cells were treated as described and then imaged on a Nikon LiveScan Swept Field Confocal Microscope (*SFC*) Eclipse *Ti* with a 60× magnification and equipped of NIS-Elements microscope imaging software (Nikon Instruments). Images were taken every 3 min with a fixed 100 ms exposure time for a total time of 30 min. PMA 10 μM was added after 3 acquisitions and the occurrence of PRKC translocation was quantified calculating the increase in fluorescence ratio with respect to time zero calculated as ratio of plasma membrane: average intracellular fluorescence.

Statistical analysis. The results were expressed as the mean ± SD and the *n* refers to the number of independent experiments. The probability of statistical differences between experimental groups was determined by the Student's t-test.

Disclosure of Potential Conflicts of Interest

No potential conflicts of interest were disclosed.

Acknowledgments

This research was supported by the Italian Association for Cancer Research (AIRC) to C.G. and P.P., Telethon (GGP09128 and GGP11139B), local funds from the University of Ferrara, the Italian Ministry of Education, University and Research (COFIN, FIRB and Futuro in Ricerca), the Italian Cystic Fibrosis Research Foundation to P.P. and Italian Ministry of Health to A.R. and P.P. S.P. is supported by a research fellowship FISM—Fondazione Italiana Sclerosi Multipla—cod. 2012/B/11; S.M. was supported by a FIRC fellowship. We thank all members of the Pinton Lab for stimulating discussion.

Supplemental Materials

Supplemental materials may be found here:
www.landesbioscience.com/journals/autophagy/article/25239

References

1. Mizushima N, Komatsu M. Autophagy: renovation of cells and tissues. Cell 2011; 147:728-41; PMID:22078875; http://dx.doi.org/10.1016/j.cell.2011.10.026
2. Levine B, Kroemer G. Autophagy in the pathogenesis of disease. Cell 2008; 132:27-42; PMID:18191218; http://dx.doi.org/10.1016/j.cell.2007.12.018
3. Bernales S, Schuck S, Walter P. ER-phagy: selective autophagy of the endoplasmic reticulum. Autophagy 2007; 3:285-7; PMID:17351330
4. Wang K, Klionsky DJ. Mitochondria removal by autophagy. Autophagy 2011; 7:297-300; PMID:21252623; http://dx.doi.org/10.4161/auto.7.3.14502
5. Kondo Y, Kondo S. Autophagy and cancer therapy. Autophagy 2006; 2:85-90; PMID:16874083
6. Sinha S, Levine B. The autophagy effector Beclin 1: a novel BH3-only protein. Oncogene 2008; 27(Suppl 1):S137-48; PMID:19641499; http://dx.doi.org/10.1038/onc.2009.51
7. Ogier-Denis E, Codogno P. Autophagy: a barrier or an adaptive response to cancer. Biochim Biophys Acta 2003; 1603:113-28; PMID:12618311
8. Arico S, Petiot A, Bauvy C, Dubbelhuis PF, Meijer AJ, Codogno P, et al. The tumor suppressor PTEN positively regulates macroautophagy by inhibiting the phosphatidylinositol 3-kinase/protein kinase B pathway. J Biol Chem 2001; 276:35243-6; PMID:11477064; http://dx.doi.org/10.1074/jbc.C100319200
9. Maiuri MC, Criollo A, Tasdemir E, Vicencio JM, Tajeddine N, Hickman JA, et al. BH3-only proteins and BH3 mimetics induce autophagy by competitively disrupting the interaction between Beclin 1 and Bcl-2/Bcl-X(L). Autophagy 2007; 3:374-6; PMID:17438366
10. Martiny-Baron G, Fabbro D. Classical PKC isoforms in cancer. Pharmacol Res 2007; 55:477-86; PMID:17548205; http://dx.doi.org/10.1016/j.phrs.2007.04.001
11. Pinton P, Rizzuto R. p66Shc, oxidative stress and aging: importing a lifespan determinant into mitochondria. Cell Cycle 2008; 7:304-8; PMID:18235239; http://dx.doi.org/10.4161/cc.7.3.5360
12. Chen JL, Lin HH, Kim KJ, Lin A, Forman HJ, Ann DK. Novel roles for protein kinase Cdelta-dependent signaling pathways in acute hypoxic stress-induced autophagy. J Biol Chem 2008; 283:34432-44; PMID:18836180; http://dx.doi.org/10.1074/jbc.M804239200
13. Sakaki K, Wu J, Kaufman RJ. Protein kinase Ctheta is required for autophagy in response to stress in the endoplasmic reticulum. J Biol Chem 2008; 283:15370-80; PMID:18356160; http://dx.doi.org/10.1074/jbc.M710209200
14. Jiang H, Cheng D, Liu W, Peng J, Feng J. Protein kinase C inhibits autophagy and phosphorylates LC3. Biochem Biophys Res Commun 2010; 395:471-6; PMID:20398630; http://dx.doi.org/10.1016/j.bbrc.2010.04.030
15. Silva RD, Manon S, Gonçalves J, Saraiva L, Côrte-Real M. Modulation of Bax mitochondrial insertion and induced cell death in yeast by mammalian protein kinase Cα. Exp Cell Res 2011; 317:781-90; PMID:21172347; http://dx.doi.org/10.1016/j.yexcr.2010.12.001
16. Chen JL, Lin HH, Kim KJ, Lin A, Ou JH, Ann DK. PKC delta signaling: a dual role in regulating hypoxic stress-induced autophagy and apoptosis. Autophagy 2009; 5:244-6; PMID:19098423; http://dx.doi.org/10.4161/auto.5.2.7549
17. Mellor H, Parker PJ. The extended protein kinase C superfamily. Biochem J 1998; 332:281-92; PMID:9601053
18. Steinberg SF. Structural basis of protein kinase C isoform function. Physiol Rev 2008; 88:1341-78; PMID:18923184; http://dx.doi.org/10.1152/physrev.00034.2007
19. Rosse C, Linch M, Kermorgant S, Cameron AJ, Boeckeler K, Parker PJ. PKC and the control of localized signal dynamics. Nat Rev Mol Cell Biol 2010; 11:103-12; PMID:20094051; http://dx.doi.org/10.1038/nrm2847
20. Giorgi C, Agnoletto C, Baldini C, Bononi A, Bonora M, Marchi S, et al. Redox control of protein kinase C: cell- and disease-specific aspects. Antioxid Redox Signal 2010; 13:1051-85; PMID:20136499; http://dx.doi.org/10.1089/ars.2009.2825
21. Kowalczyk JE, Kawalec M, Beręsewicz M, Dębski J, Dadlez M, Zabłocka B. Protein kinase C beta in postischemic brain mitochondria. Mitochondrion 2012; 12:138-43; PMID:21704734; http://dx.doi.org/10.1016/j.mito.2011.06.002
22. Lin G, Brownsey RW, MacLeod KM. Regulation of mitochondrial aconitase by phosphorylation in diabetic rat heart. Cell Mol Life Sci 2009; 66:919-32; PMID:19153662; http://dx.doi.org/10.1007/s00018-009-8696-3
23. Nunnari J, Suomalainen A. Mitochondria: in sickness and in health. Cell 2012; 148:1145-59; PMID:22424226; http://dx.doi.org/10.1016/j.cell.2012.02.035
24. Giorgi C, Agnoletto C, Bononi A, Bonora M, De Marchi E, Marchi S, et al. Mitochondrial calcium homeostasis as potential target for mitochondrial medicine. Mitochondrion 2012; 12:77-85; PMID:21798374; http://dx.doi.org/10.1016/j.mito.2011.07.004
25. Schapira AH. Mitochondrial diseases. Lancet 2012; 379:1825-34; PMID:22482939; http://dx.doi.org/10.1016/S0140-6736(11)61305-6
26. Wallace DC, Fan W, Procaccio V. Mitochondrial energetics and therapeutics. Annu Rev Pathol 2010; 5:297-348; PMID:20078222; http://dx.doi.org/10.1146/annurev.pathol.4.110807.092314
27. Gomes LC, Di Benedetto G, Scorrano L. During autophagy mitochondria elongate, are spared from degradation and sustain cell viability. Nat Cell Biol 2011; 13:589-98; PMID:21478857; http://dx.doi.org/10.1038/ncb2220
28. Vives-Bauza C, Zhou C, Huang Y, Cui M, de Vries RL, Kim J, et al. PINK1-dependent recruitment of Parkin to mitochondria in mitophagy. Proc Natl Acad Sci U S A 2010; 107:378-83; PMID:19966284; http://dx.doi.org/10.1073/pnas.0911187107
29. Mizushima N, Yoshimori T, Levine B. Methods in mammalian autophagy research. Cell 2010; 140:313-26; PMID:20144757; http://dx.doi.org/10.1016/j.cell.2010.01.028
30. Mizushima N, Yoshimori T. How to interpret LC3 immunoblotting. Autophagy 2007; 3:542-5; PMID:17611390
31. Kabeya Y, Mizushima N, Ueno T, Yamamoto A, Kirisako T, Noda T, et al. LC3, a mammalian homologue of yeast Apg8p, is localized in autophagosome membranes after processing. EMBO J 2000; 19:5720-8; PMID:11060023; http://dx.doi.org/10.1093/emboj/19.21.5720
32. Klionsky DJ, Abdalla FC, Abeliovich H, Abraham RT, Acevedo-Arozena A, Adeli K, et al. Guidelines for the use and interpretation of assays for monitoring autophagy. Autophagy 2012; 8:445-544; PMID:22966490; http://dx.doi.org/10.4161/auto.19496
33. Komatsu M, Waguri S, Koike M, Sou YS, Ueno T, Hara T, et al. Homeostatic levels of p62 control cytoplasmic inclusion body formation in autophagy-deficient mice. Cell 2007; 131:1149-63; PMID:18083104; http://dx.doi.org/10.1016/j.cell.2007.10.035
34. Komatsu M. Potential role of p62 in tumor development. Autophagy 2011; 7:1088-90; PMID:21617386; http://dx.doi.org/10.4161/auto.7.9.16474
35. Kimura S, Noda T, Yoshimori T. Dissection of the autophagosome maturation process by a novel reporter protein, tandem fluorescent-tagged LC3. Autophagy 2007; 3:452-60; PMID:17534139
36. Gonindard C, Bergonzi C, Denier C, Sergheraert C, Klaebe A, Chavant L, et al. Synthetic hispidin, a PKC inhibitor, is more cytotoxic toward cancer cells than normal cells in vitro. Cell Biol Toxicol 1997; 13:141-53; PMID:9088624; http://dx.doi.org/10.1023/A:1007321227010
37. Pinton P, Rimessi A, Marchi S, Orsini F, Migliaccio E, Giorgio M, et al. Protein kinase C beta and prolyl isomerase 1 regulate mitochondrial effects of the life-span determinant p66Shc. Science 2007; 315:659-63; PMID:17272725; http://dx.doi.org/10.1126/science.1135380
38. Rimessi A, Rizzuto R, Pinton P. Differential recruitment of PKC isoforms in HeLa cells during redox stress. Cell Stress Chaperones 2007; 12:291-8; PMID:18229448; http://dx.doi.org/10.1379/CSC-211.1
39. Takahashi H, Namiki H. Mechanism of membrane redistribution of protein kinase C by its ATP-competitive inhibitors. Biochem J 2007; 405:331-40; PMID:17373912; http://dx.doi.org/10.1042/BJ20070299
40. Soh JW, Weinstein IB. Roles of specific isoforms of protein kinase C in the transcriptional control of cyclin D1 and related genes. J Biol Chem 2003; 278:34709-16; PMID:12794082; http://dx.doi.org/10.1074/jbc.M302016200
41. Fleury C, Mignotte B, Vayssière JL. Mitochondrial reactive oxygen species in cell death signaling. Biochimie 2002; 84:131-41; PMID:12022944; http://dx.doi.org/10.1016/S0300-9084(02)01369-X
42. Marchi S, Giorgi C, Suski JM, Agnoletto C, Bononi A, Bonora M, et al. Mitochondria-ros crosstalk in the control of cell death and aging. J Signal Transduct 2012; 2012:329635; PMID:22175013; http://dx.doi.org/10.1155/2012/329635
43. Kroemer G, Galluzzi L, Brenner C. Mitochondrial membrane permeabilization in cell death. Physiol Rev 2007; 87:99-163; PMID:17237344; http://dx.doi.org/10.1152/physrev.00013.2006
44. Gottlieb E, Armour SM, Harris MH, Thompson CB. Mitochondrial membrane potential regulates matrix configuration and cytochrome c release during apoptosis. Cell Death Differ 2003; 10:709-17; PMID:12761579; http://dx.doi.org/10.1038/sj.cdd.4401231
45. Drago I, Pizzo P, Pozzan T. After half a century mitochondrial calcium in- and efflux machineries reveal themselves. EMBO J 2011; 30:4119-25; PMID:21934651; http://dx.doi.org/10.1038/emboj.2011.337
46. Pinton P, Rimessi A, Romagnoli A, Prandini A, Rizzuto R. Biosensors for the detection of calcium and pH. Methods Cell Biol 2007; 80:297-325; PMID:17445701; http://dx.doi.org/10.1016/S0091-679X(06)80015-4
47. Patergnani S, Suski JM, Agnoletto C, Bononi A, Bonora M, De Marchi E, et al. Calcium signaling around Mitochondria Associated Membranes (MAMs). Cell Commun Signal 2011; 9:19; PMID:21939514; http://dx.doi.org/10.1186/1478-811X-9-19
48. Pinton P, Leo S, Wieckowski MR, Di Benedetto G, Rizzuto R. Long-term modulation of mitochondrial Ca2+ signals by protein kinase C isozymes. J Cell Biol 2004; 165:223-32; PMID:15096525; http://dx.doi.org/10.1083/jcb.200311061

49. Heart E, Yaney GC, Corkey RF, Schultz V, Luc E, Liu L, et al. Ca2+, NAD(P)H and membrane potential changes in pancreatic beta-cells by methyl succinate: comparison with glucose. Biochem J 2007; 403:197-205; PMID:17181533; http://dx.doi.org/10.1042/BJ20061209
50. Akhmedov D, Braun M, Mataki C, Park KS, Pozzan T, Schoonjans K, et al. Mitochondrial matrix pH controls oxidative phosphorylation and metabolism-secretion coupling in INS-1E clonal beta cells. FASEB J 2010; 24:4613-26; PMID:20647546; http://dx.doi.org/10.1096/fj.10-162222
51. Poppe M, Reimertz C, Düssmann H, Krohn AJ, Luetjens CM, Böckelmann D, et al. Dissipation of potassium and proton gradients inhibits mitochondrial hyperpolarization and cytochrome c release during neural apoptosis. J Neurosci 2001; 21:4551-63; PMID:11426445
52. Mookherjee P, Quintanilla R, Roh MS, Zmijewska AA, Jope RS, Johnson GV. Mitochondrial-targeted active Akt protects SH-SY5Y neuroblastoma cells from staurosporine-induced apoptotic cell death. J Cell Biochem 2007; 102:196-210; PMID:17340627; http://dx.doi.org/10.1002/jcb.21287
53. Xiao D, Singh SV. p66Shc is indispensable for phenethyl isothiocyanate-induced apoptosis in human prostate cancer cells. Cancer Res 2010; 70:3150-8; PMID:20354186; http://dx.doi.org/10.1158/0008-5472.CAN-09-4451
54. Codogno P, Meijer AJ. Autophagy and signaling: their role in cell survival and cell death. Cell Death Differ 2005; 12(Suppl 2):1509-18; PMID:16247498; http://dx.doi.org/10.1038/sj.cdd.4401751
55. Cecconi F, Levine B. The role of autophagy in mammalian development: cell makeover rather than cell death. Dev Cell 2008; 15:344-57; PMID:18804433; http://dx.doi.org/10.1016/j.devcel.2008.08.012
56. Roffey J, Rosse C, Linch M, Hibbert A, McDonald NQ, Parker PJ. Protein kinase C intervention: the state of play. Curr Opin Cell Biol 2009; 21:268-79; PMID:19233632; http://dx.doi.org/10.1016/j.ceb.2009.01.019
57. Bononi A, Agnoletto C, De Marchi E, Marchi S, Patergnani S, Bonora M, et al. Protein kinases and phosphatases in the control of cell fate. Enzyme Res 2011; 2011:329098; PMID:21904669; http://dx.doi.org/10.4061/2011/329098
58. Reyland ME. Protein kinase C isoforms: Multi-functional regulators of cell life and death. Front Biosci 2009; 14:2386-99; PMID:19273207; http://dx.doi.org/10.2741/3385
59. Akar U, Ozpolat B, Mehta K, Fok J, Kondo Y, Lopez-Berestein G. Tissue transglutaminase inhibits autophagy in pancreatic cancer cells. Mol Cancer Res 2007; 5:241-9; PMID:17374730; http://dx.doi.org/10.1158/1541-7786.MCR-06-0229
60. He C, Klionsky DJ. Regulation mechanisms and signaling pathways of autophagy. Annu Rev Genet 2009; 43:67-93; PMID:19653858; http://dx.doi.org/10.1146/annurev-genet-102808-114910
61. Youle RJ, Narendra DP. Mechanisms of mitophagy. Nat Rev Mol Cell Biol 2011; 12:9-14; PMID:21179058; http://dx.doi.org/10.1038/nrm3028
62. Kim I, Rodriguez-Enriquez S, Lemasters JJ. Selective degradation of mitochondria by mitophagy. Arch Biochem Biophys 2007; 462:245-53; PMID:17475204; http://dx.doi.org/10.1016/j.abb.2007.03.034
63. Gomes LC, Scorrano L. Mitochondrial morphology in mitophagy and macroautophagy. Biochim Biophys Acta 2013; 1833:205-12; PMID:22406072; http://dx.doi.org/10.1016/j.bbamcr.2012.02.012
64. Twig G, Elorza A, Molina AJ, Mohamed H, Wikstrom JD, Walzer G, et al. Fission and selective fusion govern mitochondrial segregation and elimination by autophagy. EMBO J 2008; 27:433-46; PMID:18200046; http://dx.doi.org/10.1038/sj.emboj.7601963
65. Narendra D, Tanaka A, Suen DF, Youle RJ. Parkin is recruited selectively to impaired mitochondria and promotes their autophagy. J Cell Biol 2008; 183:795-803; PMID:19029340; http://dx.doi.org/10.1083/jcb.200809125
66. Narendra DP, Jin SM, Tanaka A, Suen DF, Gautier CA, Shen J, et al. PINK1 is selectively stabilized on impaired mitochondria to activate Parkin. PLoS Biol 2010; 8:e1000298; PMID:20126261; http://dx.doi.org/10.1371/journal.pbio.1000298
67. Rambold AS, Kostelecky B, Elia N, Lippincott-Schwartz J. Tubular network formation protects mitochondria from autophagosomal degradation during nutrient starvation. Proc Natl Acad Sci U S A 2011; 108:10190-5; PMID:21646527; http://dx.doi.org/10.1073/pnas.1107402108
68. Feliciello A, Gottesman ME, Avvedimento EV. cAMP-PKA signaling to the mitochondria: protein scaffolds, mRNA and phosphatases. Cell Signal 2005; 17:279-87; PMID:15567059; http://dx.doi.org/10.1016/j.cellsig.2004.09.009
69. Antico Arciuch VG, Alippe Y, Carreras MC, Poderoso JJ. Mitochondrial kinases in cell signaling: Facts and perspectives. Adv Drug Deliv Rev 2009; 61:1234-49; PMID:19733603; http://dx.doi.org/10.1016/j.addr.2009.04.025
70. Scarlett JL, Sheard PW, Hughes G, Ledgerwood EC, Ku HH, Murphy MP. Changes in mitochondrial membrane potential during staurosporine-induced apoptosis in Jurkat cells. FEBS Lett 2000; 475:267-72; PMID:10869569; http://dx.doi.org/10.1016/S0014-5793(00)01681-1
71. Paglin S, Lee NY, Nakar C, Fitzgerald M, Plotkin J, Deuel B, et al. Rapamycin-sensitive pathway regulates mitochondrial membrane potential, autophagy, and survival in irradiated MCF-7 cells. Cancer Res 2005; 65:11061-70; PMID:16322256; http://dx.doi.org/10.1158/0008-5472.CAN-05-1083
72. Chu CT. A pivotal role for PINK1 and autophagy in mitochondrial quality control: implications for Parkinson disease. Hum Mol Genet 2010; 19(R1):R28-37; PMID:20385539; http://dx.doi.org/10.1093/hmg/ddq143
73. Brown JE, Zeiger SL, Hettinger JC, Brooks JD, Holt B, Morrow JD, et al. Essential role of the redox-sensitive kinase p66shc in determining energetic and oxidative status and cell fate in neuronal preconditioning. J Neurosci 2010; 30:5242-52; PMID:20392947; http://dx.doi.org/10.1523/JNEUROSCI.6366-09.2010
74. Kleman AM, Brown JE, Zeiger SL, Hettinger JC, Brooks JD, Holt B, et al. p66(shc)'s role as an essential mitophagic molecule in controlling neuronal redox and energetic tone. Autophagy 2010; 6:948-9; PMID:20724835; http://dx.doi.org/10.4161/auto.6.7.13007
75. Bansode RR, Huang W, Roy SK, Mehta M, Mehta KD. Protein kinase C deficiency increases fatty acid oxidation and reduces fat storage. J Biol Chem 2008; 283:231-6; PMID:17962198; http://dx.doi.org/10.1074/jbc.M707268200